Impact of nitrogen availability upon the electron requirement for carbon fixation in Australian coastal phytoplankton communities

David J. Hughes[1], Deepa Varkey[2], Martina A. Doblin[1], Tim Ingleton[3], Allison Mcinnes[1], Peter J. Ralph[1], Virginie van Dongen-Vogels[1] and David J. Suggett[1*]

[1] Climate Change Cluster, University of Technology Sydney, Broadway 2007, NSW, Australia

[2]Department of Chemistry and Biomolecular Sciences, Macquarie University, NSW, Australia, 2109

[3]Waters and Coastal Science, New South Wales Office of Environment and Heritage, Department of Premier and Cabinet, Sydney, Australia

*Corresponding author: David.Suggett@uts.edu.au

Other authors: david.hughes-1@student.uts.edu.au; deepa.varkey@mq.edu.au; martina.doblin@uts.edu.au; tim.ingleton@environment.nsw.gov.au; allison.mcinnes@uts.edu.au; peter.ralph@uts.edu.au; vinnie.vandongen-vogels@uts.edu.au

Abstract

Nitrogen (N) availability affects phytoplankton photosynthetic performance and regulates marine primary production (MPP) across the global coast and oceans. Bio-optical tools including Fast Repetition Rate fluorometry (FRRf) are particularly well suited to examine MPP variability in coastal regions subjected to dynamic spatio-temporal fluctuations in nutrient availability. FRRf determines photosynthesis as an electron transport rate through Photosystem II (ETR_{PSII}), requiring knowledge of an additional parameter, the electron requirement for carbon fixation (K_C), to retrieve rates of CO_2-fixation. K_C strongly depends upon environmental conditions regulating photosynthesis, yet the importance of N-availability to this parameter has not been examined. Here, we use nutrient bioassays to isolate how N (relative to other macronutrients P, Si) regulates K_C of phytoplankton communities from the Australian coast during summer, when N-availability is often highly variable. K_C consistently responded to N-amendment, exhibiting up to a threefold reduction and hence an increase in the extent with which electrons were used to drive C-fixation. However, the process driving this consistent reduction was dependent upon initial conditions. When diatoms dominated assemblages and N was undetectable (e.g. post bloom), K_C decreased predominantly via a physiological adjustment of the existing community to N-amendment. Conversely, for mixed assemblages, N-addition achieved a similar reduction in K_C through a change in community structure towards diatom domination. We generate new understanding and parameterisation of K_C that is particularly critical to advance how FRRf can be applied to examine C-uptake throughout the global ocean where nitrogen availability is highly variable and thus frequently limits primary productivity.

Introduction

Phytoplankton are responsible for the majority of marine primary production (MPP) that fuels ocean ecosystem and climate-relevant biogeochemical cycles (Field et al. 1998; Falkowski et al. 2004). Predicting how MPP varies over space and time has therefore remained a key goal for oceanographers for over a century, but is still subject to considerable uncertainty (Laufkötter et al. 2015). This is due to a chronic lack of in-situ observational data to support predictive models, particularly for coastal waters, sub-tropical regions and the temperate southern hemisphere (Carr et al. 2006; Cheah et al. 2011; Everett and Doblin, 2015). Many studies using targeted nutrient addition bioassays (e.g. Moore et al. 2008; Tamminen and Andersen, 2007; Quigg et al. 2011) have collectively and repeatedly demonstrated that MPP is often constrained by availability of nitrogen (N) across large parts of the coastal waters and oceans around the globe (Moore et al. 2013). Hence, N supply is considered a key regulator of MPP variability.

Inorganic N is fundamental for the synthesis of proteins and nucleic acids, and critical for photoautotrophs as a key constituent of the major light-harvesting pigment chlorophyll-a (Chl-*a*), protein-rich electron transport components, and key enzymes such as ribulose bisphosphate carboxylase/oxygenase (RuBisCo), which together underpin photosynthetic electron transport and carbon (C) fixation. N-deprivation reduces photosynthetic light-harvesting efficiency due to loss of Chl-*a* and the concurrent upregulation of photoprotective carotenoid pigment synthesis (Laws et al. 1980; Rhiel et al. 1986). Photochemical efficiency of harvested light is also impaired as cells express reduced capacity for the synthesis of critical proteins (Berges et al. 1996). For example, Photosystem II (PSII), the core complex responsible for splitting water to generate electrons for photochemistry is particularly vulnerable to N deprivation, with the reaction centre protein, D1, and core antenna protein, CP47, both showing disproportionately higher losses relative to other cytoplasmic proteins

(Kolber et al. 1998). As such, N-availability directly limits photosynthesis at the cellular physiological level.

Phytoplankton communities overcome N limitation by exploiting different forms of available N. Diatoms generally dominate nitrate (NO_3^-)-rich ocean systems (Sarthou et al. 2005), possessing (i) unique combinations of nutrient assimilation pathways within their genomes (Prihoda et al. 2012), (ii) an efficient active transport mechanism for NO_3^- uptake (Falkowski, 1975), (iii) an ability to rapidly reallocate transcription profiles to incorporate N (Alexander et al. 2015), and (iv) a large internal storage vacuole permitting luxury nutrient accumulation beyond immediate growth requirements (Raven, 1997). Diatoms can thus withstand long-term N-deprivation, yet respond rapidly to newly-available NO_3^-. Loss of NO_3^- from surface waters ultimately favours smaller cells better suited to nutrient-limited conditions, whereby a larger surface area-to-volume ratio facilitates nutrient acquisition (Chisholm, 1992; Raven, 1998) or significant genome reduction to reduce cellular demand for N and Phosphorus (P) (e.g. *Prochlorococcus*) (Dufresne et al. 2003), or both. Smaller cells generally dominate in low-nutrient highly-stratified waters where regenerated forms of N such as ammonium (NH_4^+) and dissolved organic-N compounds prevail (Dugdale and Goering, 1967), with the notable exception of diazotrophs that can proliferate in N-depleted waters by fixing dissolved atmospheric N_2 (Foster et al. 2011). Nutrient injections from advection, upwelling, atmospheric deposition and coastal run off therefore stimulates new production, and progressively shifts communities away from a tightly-coupled microbial loop dominated by picophytoplankton towards taxa with greater nutrient requirements including *Synechoccocus*, and larger eukaryotes (Moore et al. 2008), with the latter cells increasing the potential for net carbon export into deep ocean waters (McAndrew et al. 2007). Such selective stimulation of large cells by transient nutrient injections is frequently observed in both open ocean (Villareal et al. 2012), and coastal waters (Wilkerson et al. 2006; Giraud et

al. 2016), leading to disproportionately productive blooms of phytoplankton and inherent variability in measured MPP rates (Kilops and Kilops, 1993).

Nutrient inputs to coasts and oceans are universally characterised by a high degree of spatial (from several kilometres to entire regions) and temporal (from hours to seasonal) variability. Coastal regions are especially subject to continuously changing physical conditions, creating a highly-dynamic nutrient and light environment for phytoplankton (Cullen et al. 2002), large variability in photosynthetic rates (Finkel and Irwin, 2000; Irwin et al. 2006) and frequent but transient blooms (Lancelot,1983; Muller-Karger et al. 2004). Reliably estimating MPP for coastal regions remains extremely challenging due to limited mechanistic (or predictive) understanding of the environmental and physiological controls regulating MPP (Moore et al. 2006) and the large gaps in data to validate primary productivity models. Satellite-based assessments of primary productivity using ocean colour are not easily applied to shallow coastal regions due to interference from coloured dissolved organic matter (CDOM), suspended sediment and land interference (Moreno-Madriñán and Fischer, 2013). Consequently, MPP estimates for coastal regions still rely largely upon direct, incubation-based measurements, which lack the spatial and temporal coverage needed to capture transient phenomena which are typical for physically-dynamic waters (see Cloern et al. 2014).

Advanced bio-optical techniques, particularly Fast Repetition Rate fluorometry (FRRf, Kolber et al. 1998, Table 1), have become important tools in resolving complex patterns of MPP variability within highly-dynamic coastal waters (e.g. Moore et al. 2003; Robinson et al. 2014) and open ocean environmental gradients (e.g. Behrenfeld et al. 2006, Suggett et al. 2006, Schuback et al. 2015, 2016, 2017). FRRf can probe photosynthetic rates in-situ near-instantaneously enabling deployment on a range of platforms and overcoming data-resolution constraints inherent with conventional incubation-based MPP measurements.

FRRf quantifies photosynthetic rates as an electron transport rate (ETR) through PSII, and not in units of C-uptake, thus requiring a conversion factor to derive FRRf-based estimates of C-fixation (Kolber and Falkowski, 1993, Moore et al. 2003, Lawrenz et al. 2013; Robinson et al. 2014). However, this conversion factor, termed the "electron requirement for carbon fixation", K_C) appears highly variable, reflecting dynamic processes which regulate the efficiency with which ETR_{PSII} is ultimately incorporated into fixed, organic C (Suggett et al. 2009a). Under physiologically "optimum" conditions for photosynthesis, linear electron flow, which generates the energy and reductant for the Calvin cycle, dominates and thus electrons are closely-coupled to C-fixation; a theoretical minimum value for K_C is generally accepted to be 4-6 mol e^- [mol C]$^{-1}$ (Genty et al. 1989; Suggett et al. 2009a). However, under less-optimal conditions, e.g. high light or nutrient limitation where the influx of electrons may exceed cellular C-fixation capacity, upregulation of electron-consuming processes other than the Calvin cycle may decouple ETR_{PSII} from C-fixation, significantly increasing K_C to values >50 mol e^- [mol C]$^{-1}$ (see Lawrenz et al. 2013). Notable processes may include alternative electron flows such as cyclic electron flow around PSII, Mehler-type reactions and alternative oxidase activity which provide sinks for excess electrons and may contribute to the activation of non-photochemical quenching (NPQ) to protect PSII from photodamage (e.g. Nawrocki et al. 2015). Growing evidence also suggests that K_C fundamentally varies as a function of the prevailing taxa (Suggett et al. 2009a; Robinson et al. 2014) in addition to environmental conditions (Lawrenz et al. 2013; Schuback et al. 2015, 2017; Zhu et al. 2016).

A recent meta-analysis encompassing >10 yr of FRRf retrieved K_C values reported broad correlations between K_C and nutrient availability (Lawrenz et al. 2013), yet was not able to isolate the specific influence of any single environmental factor and/or phytoplankton taxa upon K_C variability. Schuback et al. (2016) recently demonstrated, both observationally and experimentally, that the availability of dissolved iron (Fe) exerts a strong regulatory

146 influence on K_C; however, whether N-availability also controls this important parameter
147 remains untested. We therefore examined K_C under simulated nutrient injection scenarios by
148 performing a series of controlled, multi-factorial macronutrient bioassay experiments (N, P
149 and Silicate [Si]), upon phytoplankton assemblages collected from a dynamic coastal system
150 (Port Hacking 100 m mooring [PH_{100m}], NSW, Australia: 34.120ºS 151.224ºE). This site is a
151 well-studied coastal time-series station exhibiting seasonal dynamics in macronutrient
152 availability, with N, P and Si concentrations lowest during austral summer (December-
153 February) (Fig. 1), yet is subject to episodic uplift of nutrient-rich water due to the
154 encroachment of the proximal East Australian Current (EAC) close to the shelf (Cresswell,
155 1994; Roughan and Middleton, 2002). Phytoplankton assemblages at PH_{100m} are regularly
156 dominated by diatoms (Thompson et al. 2009; Ajani et al. 2014), thus routine episodic
157 nutrient enrichment may conceivably play an important role in the transient relief of N-
158 limitation during summer. We specifically tested the hypothesis that N-addition to
159 phytoplankton assemblages at PH_{100m} consistently reduces K_C by alleviating physiological
160 stress on their photosynthetic apparatus.
161
162 **Materials and Methods**
163 Nutrient addition bioassays were performed monthly in austral summer (December 2014 –
164 February 2015) using phytoplankton assemblages collected from the PH_{100m} coastal reference
165 station.
166 *Sampling and experimental setup* - 60 L of surface water (0-5 m depth) was collected
167 during mid-morning via repeated casts of a 10 L Niskin bottle and transferred to three 20L
168 Nalgene polyethylene carboys (Thermo-Fischer Scientific, Scoresby, Australia) and covered
169 with shade-cloth. Carboys were then transported to the laboratory within 2 hours and
170 transferred to 24x 2 L Nalgene polycarbonate bottles (Thermo-Fischer Scientific, Scoresby,

Australia), triple rinsing each bottle during the process. Filled bottles were assigned (in triplicate) as initial (unamended "time zero"), control (unamended "time final") and nutrient treatments, with one complete treatment set filled per carboy. No screening out of micro- or mesozooplankton was performed. Therefore nutrients were then added to the treatment bottles at final concentrations of 30 µM NH_4NO_3, 2 µM NaH_2PO_4 and 30 µM Na_2SiO_3 in the following combinations: +N, +P, +Si, +NP, +NSi, +PSi, +NPSi. This allowed for N to be evaluated as a potential limiting nutrient relative to both P and Si, because historically at PH_{100m} low N availability during austral summer is accompanied by low availability of other macronutrients (Fig 1). Nutrient concentrations were chosen to ensure saturated uptake rates and stimulation of primary productivity as per Quigg et al. (2011).

Bioassay incubations were performed in a temperature-controlled growth room, mimicking natural conditions for temperature, photoperiod and light quality, with light provided by T5 fluorescence tubes with a modified spectral transmission via blue filters (#172 Lagoon Blue, Lee Filters, Andover, UK), providing 100±15 µmol photons m^{-2} s^{-1}, as a conservative approximation of the daily light regime, for a total duration of 60 hours. The choice of incubation length, which inherently represents an unavoidable trade-off between minimising bottle effects yet simultaneously maximising signal-to-noise ratio (Andersen et al. 2007), was based upon a preliminary experiment performed in November 2013, where measurable physiological and taxonomic responses were observed within this timeframe (not shown). Treatment bottles were periodically inverted several times each day by hand to prevent the build-up of gas gradients. Upon termination of the experiment, water from each bottle was subsampled and allocated for: FRRf measurements, ^{14}C-uptake, Chl-*a* analysis and taxonomic identification.

Fast Repetition Rate fluorometry (FRRf)– An FRRf (FastOcean MKIII, S/N: 12-8679-007) docked with a FastACT laboratory base unit (Chelsea Technologies Group Ltd,

London, UK) was used to assess dark-acclimated photophysiology and measure electron transport rate (ETR_{PSII}). The FRRf was programmed to deliver single turnover (ST) inductions of PSII via 100 flashlets of 1 µs, spaced at 2 µs intervals delivered from a blue excitation LED (450 nm). Measurements were taken as the average of 40 sequences, with 150 ms intervals between ST acquisitions. Each ST fluorescence transient was fitted to the biophysical model of Kolber et al. (1998) using FastPro Software v1.5.2 (Chelsea Technologies Group Ltd, London, UK) to retrieve values for the minimum (F_0, F') and maximum fluorescence (F_m, F_m'), functional absorption cross section of PSII (σ_{PSII}, σ_{PSII}') and PSII connectivity factor (ρ, ρ') (where the prime notation denotes that samples were measured during exposure to actinic light). The software was also used to subtract baseline fluorescence (determined from samples gently filtered through a 0.2 µm disposable syringe filter) from the total variable fluorescence signal.

Physico-chemical parameters - Monthly sampling as part of Australia's Integrated Marine Observing System (IMOS) program determined conductivity, temperature and depth collected from Conductivity-Temperature-Depth (CTD) casts (SeaBird SBE19+, Seabird Electronics, USA). Water samples were also collected by IMOS for analysis of macronutrients (NO_3^-, ammonium, P and Si), salinity, temperature and dissolved inorganic carbon (DIC), for which data were later made publicly available via the IMOS ocean data portal (http://imos.aodn.org.au).

Carbon fixation (^{14}C- uptake)— Volumetric rates of C-fixation were determined from short-term ^{14}C-uptake incubations, where 50 mL subsamples from treatment bottles were transferred to 75 mL culture flasks (Sigma-Aldrich Pty Ltd, Castle Hill, Australia) and spiked with 20 µCi $NaH^{14}CO_3$ (Perkin-Elmer, Melbourne, Australia) to a final activity of ~0.4 µCi mL^{-1}. Total activity was determined from 150 µL aliquots which were immediately removed and fixed with 10 mL scintillation fluid (Ultima Gold LLT, Perkin-Elmer) before subsequent

liquid scintillation counting (Tri-Carb 2810 TR, Perkin-Elmer). Spiked samples were incubated under the experimental setup described above for 2 hours. For all months, samples were incubated in three batches (i.e. one triplicate from each treatment together with a control) at: morning, mid-day and early afternoon. Following incubation, sample flasks were immediately put on ice in total darkness. Samples were then filtered under gentle vacuum through Whatman GF/F filters, acidified with 150 µL of HCl (6 M) to drive remaining unfixed C to CO_2 and degassed overnight before fixation with 10 mL scintillation fluid. For blank determination (T^O), 50 mL was pooled from each set of triplicate treatment bottles, spiked as before, then immediately filtered and acidified before following the degassing and fixing procedure. Fixed samples were shaken vigorously for 2 minutes then subjected to liquid scintillation counting to measure disintegrations per minute (DPM), subsequently converted to units of C fixation (mg C m^{-3} hr^{-1}) as per Knap et al. (1996). DIC concentration was sourced from the IMOS online data repository (http://www.imos.org.au/), and an isotopic discrimination factor of 1.05 was used (Welschmeyer et al. 1984).

FRRf electron transport rate - Samples were kept under very low light (~2-3 µmol photons m^{-2} s^{-1}) for 20 minutes prior to FRRf measurements to NPQ processes, whilst minimising any potential build-up of chlororespiration that can occur during dark-acclimation (Kromkamp and Forster, 2003). Aliquots of 3 mL from each treatment bottle were transferred to Pyrex test tubes and loaded into the FRRf optical head, housing a white actinic LED programmed to deliver continuous irradiance (100 µmol photons m^{-2} s^{-1}, as per bioassay conditions) for a period of 6 minutes. The photosynthetic electron transport rate ($ETR_{PSII,}$ electrons m^{-3} s^{-1}) was determined using the biophysical "sigma-based" algorithm originally developed by Kolber and Falkowski (1993).

$$\mathbf{ETR_{PSII}} = E \cdot \sigma_{PSII}' \cdot (1/[F_v/F_m]) \cdot [RCII]^{(FRRf)} \cdot (1\text{-}C) \cdot 2.167 \cdot 10^3 \quad (1)$$

where E is irradiance (µmol photons m^{-2} s^{-1}), σ_{PSII}' is the functional absorption cross-section of PSII under actinic light (nm^{-2} $quanta^{-1}$), $[RCII]^{(FRRf)}$ is the concentration of PSII reaction centres (mol RCII m^{-3}) estimated fluorometrically according to Oxborough et al. (2012):

$$[\mathbf{RCII}]^{(\mathbf{FRRf})} = \frac{K_R}{E_{LED}} \times \frac{F_0}{\sigma_{PSII}} \quad (2)$$

where K_R is an instrument-specific constant (photons m^{-3} s^{-1}) and E_{LED} is the intensity of the fluorometer's 450 nm measuring beam (photons m^{-2} s^{-1}). We note that this algorithm has since been modified by Murphy et al. (2017), substituting F_0/σ_{PSII} for $F_0'_{OXBO}/\sigma_{PSII}'$ (where $F_0'_{OXBO}$ is calculated as per Oxborough and Baker, 1997) to account for effects of photoinactivation and chlororespiration on F_0. Unfortunately, our FRRf measurement protocol did not allow for reliable estimation of σ_{PSII}' in the absence of non-photochemical quenching. We therefore calculated $F_0'_{OXBO}$ and compared this with our measured F_0 finding a near-perfect equivalence (Slope: 1.003, R^2=0.998, n = 80, Supplementary Fig. S1) suggesting that neither photoinactivation, nor chlororespiration, impacted our calculations of $[RCII]^{(FRRf)}$. As such, it is unlikely that the Murphy et al. (2017) modifications would have helped to improve $[RCII]^{(FRRf)}$ retrieval during this study. Here, we specifically use the superscript $^{(FRRf)}$ to differentiate estimates of PSII reaction centres using fluorescence data, rather than conventional oxygen flash-yield methodology for which we reserve the term [RCII]. The fraction of [RCII] in the closed state is denoted by C, calculated here as 1-qP (qP = $(F'-F_0')/(F_m'-F_0')$. The inclusion of the factor $1/[F_v'/F_m']$ (where $F_v'/F_m' = [F_m' - F_0']/F_m'$) accounts for the non-radiative loss of energy associated with σ_{PSII}' (Kolber et al. 1998; Suggett et al. 2009a; Oxborough et al. 2012). Both [RCII] and (1-C) are necessary in

order to measure gross photosynthesis (Kolber and Falkowski, 1993). Inclusion of the constant 2.167 x 10^3 accounts for the conversion of µmol photons to photons, nm^2 to m^2, quanta to mol [RCII] and seconds to hours, yielding ETR_{PSII} with units of electrons m^{-3} h^{-1}, assuming an efficiency of one charge-separation event per photon absorbed (see Kolber and Falkowski, 1993). Measurements of σ_{PSII}' are spectrally-weighted towards the FRRf excitation LED (450 nm) and thus were spectrally-adjusted using a correction factor based on the dominant taxonomic group present in the sample (usually diatoms), identified by microscopy. For this we used previously-collected fluorescence excitation spectra (400-700 nm) from phytoplankton cultures pre-treated with 3-(3,4-dichlorophenyl)-1,1-dimethylurea (DCMU) where fluorescence emission was measured at 730 nm (see Suggett et al. 2009b; Wu et al. 2014) to obtain spectrally resolved values of PSII effective absorption, $\sigma_{PSII}'(\lambda)$ as,

$$\boldsymbol{\sigma_{PSII}}'(\boldsymbol{\lambda}) = \left(\boldsymbol{\sigma_{PSII}}'(\mathbf{450}) \Big/ \boldsymbol{F_{730}}(\mathbf{450}) \right) . \boldsymbol{F_{730}}(\boldsymbol{\lambda}) \qquad (\mathbf{3})$$

Values of $\sigma_{PSII}'(\lambda)$ were then spectrally-adjusted to the actinic light source within the FRRf optical head as,

$$\overrightarrow{\boldsymbol{\sigma_{PSII}}'} = \left(\sum_{\mathbf{400}}^{\mathbf{700}} \boldsymbol{\sigma}_{\mathbf{PSII}}^{'(\lambda)} . \boldsymbol{E}(\boldsymbol{\lambda}) \right) \Delta\boldsymbol{\lambda} \Big/ \sum_{\mathbf{400}}^{\mathbf{700}} \boldsymbol{E}(\boldsymbol{\lambda}) \Delta\boldsymbol{\lambda} \qquad (\mathbf{4})$$

ETR_{PSII} was measured every 10 seconds during the 6 minute incubation period; however we report the integrated rate over the final minute of the incubation period which we consider representative of steady-state electron transport (see Suggett et al. 2009a). All FRRf

incubations were performed in batches of triplicates and randomised with time of day, over the daylight period.

$$\mathbf{ETR_{PSII}} = \left(\sum_{t(start)}^{t(end)} \mathbf{ETR_{PSII}}\,(t)\Delta t \right) . \left({}^{60}/_{\sum t} \right) \quad (5)$$

A further correction factor was then applied to account for spectral differences between the FRRf actinic light source and the actinic light source driving the ^{14}C-uptake incubation. Here, we measured the spectral output of the blue-filtered fluorescent tubes used for the ^{14}C-incubations using a spectrometer system (JAZ, Ocean Optics, Florida, USA). ^{14}C-uptake rates were then corrected to correspond with the FRRF's white LED spectrum as per Suggett et al. (2001) for direct comparison against measured ETR_{PSII}.

Non-photochemical quenching - NPQ was calculated as the normalised Stern-Volmer coefficient (thus denoted here as NPQ_{NSV}) as per Oxborough (2012):

$$\mathbf{NPQ_{NSV}} = \mathbf{1} / \left(\frac{F_v'}{F_m'} \right) - \mathbf{1} \quad (6)$$

Size-fractionated Chl-a — Total Chl-*a* for all samples was determined by filtering 250 mL of seawater under gentle vacuum through a Whatman GF/F filter (0.7 µm nominal pore size) before immediate extraction of pigments in 90% acetone and storage at 4°C in darkness. For the >10 µm fraction, a similar procedure was conducted, but instead using 10 µm polycarbonate filters (Merck Millipore, Bayswater, VIC, Australia). After 48 hours of extraction in 90% acetone, Chl-*a* for all samples was determined fluorometrically using a

fluorometer (Trilogy, Turner Designs, Sunnyvale, California, USA), fitted with a Chl-*a* Non-acidification Module (Turner Design, USA), calibrated against pure Chl-*a* standards (Sigma-Aldrich Pty Ltd).

Phytoplankton taxonomy - To resolve the <10 µm taxonomic fraction, aliquots of 1.8 mL were fixed with gluteraldehyde (Sigma-Aldrich Pty Ltd) to a final concentration of 0.4%, snap-frozen in liquid N_2 and stored at -80°C. Samples were subsequently analysed within 2 months, quick-thawing for approximately 1-2 minutes at 30°C, and community structure analysed via flow-cytometry (Influx Flow Cytometer, Becton Dickinson, Australia). A known concentration of yellow-green fluorescent beads was used to standardise event counts and picophytoplankton were enumerated and classified under one of three categories: a) *Prochlorococcus*, b) *Synechococcus* or c) picoeukaryote. The sum of a) and b) was used to calculate total picocyanobacteria abundance. Larger aliquots of 250 mL were taken to resolve the >10 µm taxonomic fraction from each treatment bottle, preserved with 2% final volume alkaline Lugol's solution and stored in amber-tinted glass bottles. Samples were then concentrated by settlement for 48 hours and siphoned by gentle vacuum from the meniscus to achieve a final concentrated sample of ~25 mL. Identification and enumeration of cells was then performed using a Sedgewick-Rafter counting chamber. Cells were examined at 200x magnification and identified to genus level where possible (otherwise to at least family level). Where possible, a minimum of 100 cells was counted per sample; however, this was not always achievable in samples with relatively low biomass (where >10 µm Chl-*a* $\leq$ 1 mg m^{-3}). In such instances as many cells as possible were counted from three repeated loadings of the counting chamber (3 mL total sample analysed). All microscopy samples were analysed within 2 months from the date of being fixed.

Statistical analysis - One-way analysis of variance (ANOVA) was used to determine statistical relationships between bioassay treatments, with Dunnett's post-hoc method to

compare all nutrient treatments against the control ($p < 0.05$), and Tukey's HSD all-pairwise comparison to evaluate differences between triplicate carboys. Normality and homogeneity of variance were verified using Shapiro-Wilk's and Levene's tests respectively. All statistical analyses were performed using SigmaPlot v12.0 (Systat Software Inc, California, USA).

Results

Initial conditions - For all three bioassays, initial nutrient concentrations were generally low. Initial NO_3^- concentrations were below the limit of detection (<0.05 µmol L^{-1}) for December and February, but not for January where NO_3^- was 0.1 µmol L^{-1} (Table 2). Phosphate (PO_4^{3-}) concentrations were ~0.15 µmol L^{-1} for both January and February, but were twice as low for December (0.07 µmol L^{-1}) (Table 2). Initial Si concentrations were 0.7 and 0.5 µmol L^{-1} during December and January respectively, but below the detection limit (<0.1 µmol L^{-1}) for February (Table 2). Overall, these macronutrient concentrations fell within the expected range of values for austral summer, based on historical data (Fig. 1). Sea surface temperature (SST) increased from 21.6ºC in December, to over 23 ºC in both January and February (Fig. 2, Table 2). Dissolved organic carbon (DIC), together with salinity showed little variation between months, while mixed layer depth (MLD) varied between 10 m and 25 m (Table 2).

December and February were both characterised by low overall phytoplankton biomass (0.88-2.01 mg Chl-*a* m^{-3}, Table 2), with phytoplankton cells belonging to >10 µm size fraction (dominated by diatoms, *Leptocylindrus* spp. and *Nitzschia* spp., Table 3) accounting for nearly 40% of total Chl-*a* measured (Fig 3d, f, g, i). However, the electron requirement for carbon fixation, K_C, was considerably lower for December than February (7.47 and 16.2 mol e^- [mol C]$^{-1}$ respectively, Fig. 3a, c). Total Chl-*a* was notably higher for January (5.24 mg m^{-3}) than for December and February, with >10 µm phytoplankton

accounting for a greater proportion of total Chl-*a* (~60%), but representing a co-dominance of diatoms (*Leptocylindrus* spp. and *Chaetoceras* spp.), and dinoflagellates (*Prorocentrum* spp. and *Protoperidinium* spp.) (Fig 3b, e, h, Table 3). K_C for January was closer to February values at 12.2 mol e^- [mol C]$^{-1}$, approximately two-fold higher than that for December (Fig. 3a-c). Picoeukaryotes formed a much larger proportion of total picophytoplankton cells in January (almost 50%), than during the other two months when abundance was an order of magnitude lower (Table 2). December initial samples exhibited the lowest values of F_v/F_m, which were accompanied by the largest measured values for σ_{PSII}' and NPQ_{NSV} (Fig. 4a, d, j). Conversely, February initial samples showed the opposite trend, with the highest measured F_v/F_m but lowest values for both σ_{PSII}' and NPQ_{NSV} (Fig. 4c, f, l). Intermediate values for F_v/F_m, σ_{PSII}' and NPQ_{NSV} were measured for January (Fig. 4b, e, k).

Response to nutrient injection— In December all N-containing treatments yielded a two-fold decrease in K_C to values of ~ 5 mol e^- [mol C]$^{-1}$ compared to the unamended control of ~8.5 mol e^- [mol C]$^{-1}$ after 60 hours (ANOVA, $p < 0.05$) (Fig. 3a). Total Chl-*a* increased for all treatments, together with the >10 µm size-fractionated Chl-*a* for the NSi and NPSi treatments (ANOVA, $p < 0.01$) (Fig 3a, d, g). A notable photophysiological response to treatments containing N was also apparent, with reductions to σ_{PSII}' and NPQ_{NSV} relative to controls (ANOVA, $p < 0.05$), and increased F_v/F_m for NSi and NPSi treatments only (ANOVA, $p < 0.01$) (Fig. 4a). Together these responses highlighted proximal relief from N-limitation, with largest responses observed for joint N and Si additions. Diatoms dominated the phytoplankton community composition for all treatments, with *Leptocylindrus* spp., *Nitzschia* spp. and *Skeletonema* spp. accounting for between 60-90% of cells (Table 3). No differences in K_C, Chl-*a* or >10 µm Chl-*a* were observed between control samples and Si, P or PSi treatments (Figure 3a, d, g). Whilst the total concentration of picophytoplankton cells remained largely constant across treatments, a two-fold decrease in cell abundance was

observed within the Si and NSi treatments (ANOVA, $p < 0.05$) (not shown). For the N and NP treatments, we observed no changes to phytoplankton size structure (Fig 3g), dominant taxonomic group (Table 3) or the number of total picophytoplankton cells during the bioassay (Fig 3j). Thus, K_C changes for this experiment can only be attributed to a physiological adjustment of the existing phytoplankton community in response to N-addition.

Nutrient addition responses for February generally followed the same trend observed for December, with most N-containing treatments (except N-only) stimulating up to a two-fold reduction in K_C (ANOVA, $p < 0.01$) from ~16 to ~8 mol e^- [mol C]$^{-1}$ (Fig 3c). However, despite this reduction, the minimum recorded value of K_C (7.8 mol e^- [mol C]$^{-1}$, for +NP treatment) was still nearly twice that measured in December for N-amended treatments. *Leptocylindrus* spp. accounted for between ~60-90% of all large cells and other diatom genera were less abundant than in previous months (Table 3). Resolving further trends in other parameters for this month proved problematic due to the large variance between triplicates, hence despite apparent trends in the data upon visual examination for both Chl-*a* and >10 µm Chl-*a*, they were statistically indistinguishable from control samples, together with other variables measured across treatments. This variance across replicates was identified to specifically stem from one of the three carboys (and hence one of the three treatment sets) containing large quantities of an unidentified nanoflagellate within the 0.2-10 µm size fraction, which contributed significantly towards total biomass, and was conspicuously absent from the other two carboys (Supplementary Figure S2). Thus overall, N appeared to be the limiting nutrient for both December and February, when N-amended treatments generally showed a strong physiological response and a largely unchanged phytoplankton community composition.

In contrast to either December or February, bioassay responses for January were markedly different since K_C decreased significantly for all nutrient treatments. Addition of N

and P alone resulted in a two-fold reduction in K_C to approximately 7 mol e^- [mol C]$^{-1}$ (ANOVA, $p < 0.05$), whilst Si, NP, NSi and PSi elicited a three-fold decrease to ~5 mol e^- [mol C]$^{-1}$, compared to the unamended control (12.3 mol e^- [mol C]$^{-1}$). Nutrient addition responses appeared to be cumulative, with NPSi addition resulting in the greatest reduction of K_C to the lowest recorded value of ~3 mol e^- [mol C]$^{-1}$. NPSi addition also stimulated a four-fold increase in Chl-*a* biomass to ~20 mg m^{-3} (the highest recorded), which was the only statistically significant Chl-*a* biomass response across all treatments for this month (ANOVA, $p < 0.01$) (Figure 3e). Diatoms continued to largely account for the >10 µm cell fraction; however, *Chaetoceros* replaced *Nitzschia* as the co-dominant genus alongside *Leptocylindrus* (Table 3). Parallel photophysiological responses highlighted a response particularly to Si- (rather than N-) via an increase in F_v/F_m, to a maximum value of 0.51 (Fig. 4c), and a decrease in NPQ_{NSV} to a minimum of 0.97 (Fig. 4k), compared to control values of 0.4 and 1.8, respectively.

Across the three months, all nutrient-amended increases in >10 µm Chl-*a* were strongly correlated to the increase in bulk Chl-*a* concentrations ($R^2 = 0.92$, not shown), confirming that overall increases in biomass were driven primarily by the response of larger cells to nutrient enrichment. Despite evidence suggesting macronutrient limitation of phytoplankton Chl-*a* concentrations (especially for N-treatments in December), few significant differences in values of F_v/F_m were observed across the three experiments (Fig 5a-c).

Discussion

FRRf-based studies have previously demonstrated that macro- (Lawrenz et al. 2013) and micro-nutrient availability (Schuback et al. 2015, 2017) are likely key regulators of the electron requirement for carbon fixation (K_C), and thus the efficiency with which photochemical energy fuels C assimilation. However, there appear to be species-specific differences in K_C, thus the phytoplankton community composition may also play an important role in the regulation of K_C (Suggett et al. 2009a; Robinson et al. 2014). Consequently, separating the effect of a nutrient-induced change in physiology, from a nutrient-induced change in taxonomic composition upon K_C has remained problematic, and perhaps unsurprising considering nutrient availability is a strong selective pressure over phytoplankton community composition itself (Tilman et al. 1982). By using a bioassay-based platform for the first time to examine nutrient stimulated changes in K_C, we provide new evidence that K_C is consistently altered by general trends in environmental nutrient availability (in our case N and Si), but through a complex combination of taxonomic and/or physiological responses to the existing community. We discuss these various responses in the following sections and how they potentially influence future FRRf-based studies of K_C in coastal waters.

Predominance of physiological relief of nutrient limitation upon K_C

Relief from N-limitation drove a reduction in K_C *in both December and February* (Fig. 3a, c), despite the high variance in February across treatments (carboy 3, see Supplementary Figure S2). The (two-fold) decrease in K_C was observed in N-containing treatments only, indicating that other macronutrients (P, Si) in isolation were not strong regulators of the coupling of electrons and carbon, i.e. K_C for the phytoplankton taxa present; however there was an additional stimulation of biomass when Si was provided in addition to N. Importantly,

these patterns reflected a physiological response to the largely unchanged taxonomic (diatom-dominated) composition. Key photophysiological responses were consistent with alleviation of N-limitation for diatoms; specifically a simultaneous decrease to the functional absorption cross-section of PSII (σ_{PSII}), increase in F_v/F_m (for NSi and NPSi) and decreased induction of non-photochemical quenching (NPQ_{NSV}) (Figs 4d, f, j, l). Parallel increases of σ_{PSII} and decreases of F_v/F_m are usually attributed to the loss of functional PSII reaction centres under N-limitation (observed in diatoms *Thalassiosira weissflogii*, *T. pseudonana* and *Skeletonema costatum*) (Kolber et al. 1998; Falkowski et al. 1992). Significant declines in F_v/F_m have been observed in laboratory batch cultures of phytoplankton upon depletion of N in the growth media including the diatoms *Phaeodactylum tricornatum* (Geider et al. 1993) and *T. weissflogii* (Berges et al. 1996). Whilst an inverse covariation between F_v/F_m and σ_{PSII} is often indicative of an underlying change in community size structure (Suggett et al. 2009b), this is clearly not the case given the combined photophysiological and taxonomic responses for December and February (Fig. 4, Table 3).

A decrease of NPQ_{NSV} is also consistent with an expected physiological response to alleviation of N-limitation: Deprivation of NO_3^- limits the rate of C-fixation, thereby reducing the capacity of a key electron sink downstream of PSII (Huner et al. 1998), potentially leading to an accumulation of excess excitation energy in a manner similar to that experienced by cells during transient high light stress. Phytoplankton must employ strategies to dissipate such excess excitation energy either *before* charge-separation as thermal dissipation (estimated here as NPQ_{NSV}), or *after* charge-separation via alternative electron flows that do not fix carbon, and therefore increase K_C (Mackey et al. 2008; Bailey et al. 2008; Cardol et al. 2011). Coastal diatoms have a particularly high capacity for NPQ, associated with a xanthophyll cycle controlled by a light-dependent trans-thylakoid proton gradient (ΔpH) (Lavaud et al. 2004; Lavaud and Kroth, 2006). Importantly, because most

alternative electron flows generate ΔpH which, in turn, activates components of NPQ (Nawrocki et al. 2015), a large increase in NPQ expression may therefore reflect a physiological stress response to N-deprivation (see White et al. 2011). Indeed, supplementation of NO_3^- to N-limited coastal assemblages dominated by the diatoms, *Thalassiosira* and *Chaetoceros* was shown to decrease NPQ (Bouchard et al. 2008). In this case, Bouchard et al. (2008) suggested that NO_3^- addition allowed cells to maintain a higher concentration of RuBisCO large sub-units, thereby increasing C-fixation capacity relative to electron transport and reducing excitation pressure on PSII. The resulting decrease in lumen acidification, would lead to a subsequent decrease of ΔpH-dependent NPQ (Wilson and Huner, 2000). Geider et al. (1993) demonstrated that the small subunit of RuBisCO is also negatively impacted by N starvation in *P. tricornutum*, which is also likely to increase excitation pressure on PSII and increase the probability of alternative electron flow. Down-regulation of alternative electron flow pathways in response to alleviation of physiological nutrient-stress in the N-amended treatments could thus potentially explain the reduction of both NPQ_{NSV} and K_C in our N-amended treatments for December (Figs. 4a, 3a.) and carboys 1-2 in February (Supplementary Figure S2). However, we note that Schuback et al. (2015) observed that NPQ_{NSV} and K_C are not entirely independent of one another, as both depend on the fluorescence parameter, F_v'. Nevertheless, it is would be highly desirable to utilise NPQ_{NSV} as a predictor of K_C in Australian coastal waters, following on from recent attempts to do so elsewhere (Schuback et al. 2015, 2016, 2017; Zhu et al. 2016). We revisit this point later in this discussion.

Diatoms have been reported with values for K_C ranging from 3-8 mol e^- [mol C]$^{-1}$ in N-replete growth under laboratory conditions (Suggett et al. 2009a; Hoppe et al. 2015). Consequently, our N-amended treatments show K_C values consistent with previous studies. To our knowledge, no study has examined K_C for phytoplankton grown under N-limited

511 conditions. Schuback et al. (2015) reported that values of K_C for *T. oceanica* cultures
512 increased under Fe-limitation; however, because their approach conflated variability of both
513 K_C and [RCII], it is necessary to use assumed values of $1/n_{PSII}$ (mol Chl-*a* [mol $RCII^{-1}$]) in
514 order to estimate their absolute change in K_C. Using values of 500 and 700 mol Chl-*a* [mol
515 $RCII^{-1}$] for Fe-replete and Fe-limited (as applied by the authors to their field dataset in the
516 same study), indicates that K_C increased from 11.7 to 13.2 mol e^- [mol C]$^{-1}$ under Fe-
517 limitation. This trend would appear to support our observations that alleviation of nutrient
518 limitation reduces K_C, and can do so purely via a physiological adjustment (i.e. with no
519 change in community composition).

520 Our data shows that the photosynthetic unit (PSU) size of PSII was often found to
521 increase due to N-amendment (Fig. 5), contrasting with Berges et al. (1996) who reported N-
522 starved *T. weissflogii* to exhibit PSU sizes nearly three-fold larger than N-replete cultures. In
523 previous studies, a loss of PSII reaction centres (RCIIs) due to a compromised D1 protein
524 repair cycle (see Prézelin et al. 1986; Bergmann et al. 2002) relative to cellular Chl-*a* was
525 responsible for this increase in PSU size under N-limitation (Berges et al. 1996; Kolber et al.
526 1988). The parallel increase in F_v/F_m and decrease of σ_{PSII} observed for N-amended
527 treatments in this study indicates that RCIIs were being repaired under N-supplementation,
528 ruling out the possibility of photoinhibition, thus an increased PSU size suggests either: the
529 fluorescence-based algorithm of $[RCII]^{(FRRf)}$ (Oxborough et al. 2012) used in our calculations
530 of ETR_{PSII} underperformed, or that the response of Chl-*a* synthesis over the timeframe of the
531 incubations exceeded the RCII repair/synthesis rate. The Oxborough et al. (2012) FRRf-
532 derived [RCII] algorithm has been used previously in Australian coastal waters (Robinson et
533 al. 2014), and has been validated for several diatom species, including Fe-limited cultures
534 (Oxborough et al. 2012; Silsbe et al. 2015; also see Murphy et al. 2017). However, no study
535 has examined how PSU size responds to the alleviation of N-limitation within a controlled

bioassay experiment. Repair rates of RCII may vary between diatom species but is generally a rapid process under low irradiance (Lavaud et al. 2016). Young and Beardall (2003) demonstrated that re-supply of N to an N-starved chlorophyte (*Dunaliella tertiolecta*) resulted in a complete recovery of F_v/F_m within 24 hours. Our experimental design did not permit the assessment of either Chl-*a* or [RCII] dynamics over the timescale of this bioassay, and conceivably the PSU size response could have been very different had we examined this after a shorter elapsed time following nutrient amendment. Diatoms have a large capacity to synthesize Chl-*a* rapidly (Owens et al. 1978), and demonstrate great structural flexibility within the chloroplast relative to other taxa (Wilhelm et al. 2006). Indeed, PSU size for diatoms has been demonstrated to vary considerably in response to irradiance levels (e.g. 553-723 for *T. weissflogii*, Dubinsky et al. 1986), increasing under both low light (Gallagher et al. 1984), and constant light (Fietz and Nicklisch, 2002). Therefore, the observed increases in PSU size could potentially be attributed to the relatively low, constant light field provided within our experimental setup. Consequently, it is plausible that use of a single light intensity, which itself may not accurately represent the light availability experienced *in situ*, is not enough to resolve some of the complexities of the bioassay responses observed within this study. As it stands, our measured changes in PSU size have implications for the interpretation of the physiological response driving the reduction in K_C for N-amended treatments:

When C-fixed and ETR_{PSII} are both normalised to Chl-*a* concentration (Fig 5g-i), reductions in K_C for December were driven mainly from a reduction in ETR_{PSII} rather than an increase in C-fixation (Fig 5g), whilst both mechanisms were responsible for lowering K_C in February. The observed reduction in ETR_{PSII} per Chl-*a* is consistent with physical constraints associated with pigment packaging effects upon light harvesting (Morel and Bricaud, 1981), which can lead to an inverse relationship between PSU size and photosynthetic efficiency per

561 Chl-*a* (Perry et al. 1981). However, the apparent insensitivity of C-fixation to N-amendment
562 we observed for December and January would appear contrary to recent studies
563 demonstrating that Chl-*a* normalised C-assimilation generally increases with N-availability
564 for diatoms (Zhao et al. 2015; Berg et al. 2017).

565 Given that we observed such a strong Chl-*a* and PSU size response for some N-
566 amended treatments (possibly linked to incubation conditions as discussed previously),
567 normalisation of ETR_{PSII} and C-fixed to Chl-*a* could potentially bias interpretation of the
568 dynamics in K_C. Indeed, when C-fixed and ETR_{PSII} are both instead normalised to [RCII]
569 concentration, our data shows that the addition of N preferentially stimulated an increase in
570 C-fixation which led to a decrease in K_C (Fig. 6a, c). Previous studies have shown that under
571 N-limitation, both the concentration, and activity of RuBisCo declines relative to electron
572 transport (Berges et al. 1996; Sciandra et al. 1997), which would support our observations.
573 Furthermore, large diatoms (e.g. *Leptocylindrus*, such as those found in assemblages during
574 this study) have been shown to invest a larger proportion of cellular N into C-fixation
575 machinery compared to small diatoms (Wu et al. 2014), meaning that the diatom assemblages
576 within this study could reasonably be expected to exhibit a strong C-fixation response to N-
577 amendment.

578 Using the Oxborough et al. (2012) algorithm to calculate ETR_{PSII} within our bioassay
579 approach demonstrates that alleviation of N-limitation reduces K_C, yet also identified
580 surprising PSU size dynamics that clearly warrant further investigation. In spite of this
581 current uncertainty, the Oxborough et al. (2012) approach (later modified by Murphy et al.
582 2017) arguably represents the best option currently available for measuring K_C, because the
583 assumption of a "fixed" n_{PSII} value (e.g. Babin et al. 1996; Smyth et al. 2004) is notoriously
584 inaccurate (Suggett et al. 2004) and represents the largest source of uncertainty in

calculations of ETR_{PSII} (Robinson et al. 2009). Further evaluation of the algorithm's robustness under variable N-availability is therefore critical for future research.

A role for taxonomy in regulating K_C?

The first evidence for taxonomic regulation of K_C was observed in the February bioassay, when measured K_C for carboy 3 (dominated by small flagellates) was consistently higher than carboys 1-2 (diatom-dominated) for all but one N-amended treatment (Supplementary Figure S2). This response is consistent with the observations of Suggett et al. (2009a) who reported a higher K_C for the flagellate, *Pycnococcus provasoli* (11.52 mol e^- [mol C]$^{-1}$) than for the diatom, *T. weissflogii* (5.37 mol e^- [mol C]$^{-1}$) under N-replete growth, providing additional evidence for the regulation of this conversion factor by taxa present.

In January, all treatments exhibited a decrease in K_C, corresponding to a taxonomic response whereby the community shifted towards diatom-domination from an initial community that was co-dominated by both diatoms and dinoflagellates. Therefore, at face value it would appear that taxonomy is driving this reduction in K_C; however, significant responses of both F_v/F_m, and NPQ_{NSV} suggest that K_C is most likely controlled by a complex mix of physiology and taxonomy for this month. Curiously, physiological responses were associated mostly with Si-addition. Whilst Si is generally considered to be a key limiting nutrient for cellular division in diatoms (Claquin et al. 2002), but not in their physiological regulation (Alexander et al. 2015), few studies actually support this broad assertion and it remains unclear why diatoms often exhibit a physiological response to Si-addition (Shrestha et al. 2012). Indeed, the observed decrease of NPQ_{NSV} in Si-amended treatments would appear to support findings by Lippemeier et al. (1999) who reported a similar downregulation of NPQ for Si-limited cultures of diatoms (*T. weisflogii*) upon re-introduction of Si to the growth media. Although the underlying mechanism was not elucidated, it was proposed that

609 Si-addition likely stimulated reversal of an increased proton gradient responsible for NPQ
610 activation though increased C-fixation capacity via two probable mechanisms: i) enhanced
611 protein synthesis over a timescale of hours and/or ii) reversal of intracellular accumulation of
612 amino acids associated with enhanced photorespiration, over a timescale of minutes. Thus,
613 our data provide additional evidence for a direct role of Si over photosynthetic performance,
614 yet because the responses were observed over a 60 h period, the underlying mechanism
615 remains unclear and warrants further testing. The markedly different bioassay response for
616 January potentially suggests relief from nutrient starvation, due to the fact that initial Chl-*a*
617 (>5 mg m^{-3}) was significantly higher than either December or February, indicating that
618 sampling occurred in the latter stages of a bloom.

619 *K_C variability induced from carbon lifetimes*

620 Whilst physiological and taxonomic adjustments provide a plausible explanation for the
621 decrease in particularly K_C nitrogen-amended treatments, we should also consider a third
622 possibility in explaining the observed trends. A potential confounding factor, which could
623 account for an apparent reduction in measured K_C values, is that stimulation of phytoplankton
624 growth rates in response to nutrient-amendment may have increased the lifetime of newly-
625 fixed carbon products (as per Halsey et al. 2010, 2011, 2013). In such a scenario, it is feasible
626 that a greater proportion of ^{14}C may be retained during a two-hour incubation period, thus
627 shifting the overall process captured by the ^{14}C method closer towards GPP. Consequently,
628 lower K_C could simply reflect a higher (i.e. closer to GPP C-fixation rate) rather than an
629 alleviation of 'photosynthetic stress' (increased efficiency of electron investment into fixed-
630 C). However, in order to identify the influence of C-lifetimes upon K_C, ultimately requires
631 time-resolved experimentation to measure exactly where a measured ^{14}C-uptake rate sits on
632 the 'sliding scale' from GPP to NPP (e.g. Milligan et al. 2015). Whilst this has been well-
633 studied in phytoplankton laboratory cultures (Halsey et al. 2010, 2011, 2013) where high

biomass permit for use of very short (e.g. <20min) ^{14}C incubations, for natural field settings where biomass is often far lower, inherent signal-to-noise constraints of ^{14}C-based approaches require lengthier incubations to reliably measure ^{14}C-uptake and thus this remains an unresolved challenge for oceanographic work. In spite of this potential alternative explanation for reductions of K_C observed during this study, the important point remains that the measured response (i.e. lower K_C to alleviation of N-limitation) holds true irrespective of the underlying mechanism by which this is ultimately achieved.

Predicting K_C from NPQ_{NSV}

As demonstrated in Fig. 6, we found a strong relationship between K_C and NPQ_{NSV} for each month individually, but to a lesser degree when all the data was pooled ($R^2 = 0.41$, $p < 0.001$, Fig 6a). In contrast, for analysis where n_{PSII} is unknown or assumed (and hence K_C/n_{PSII}, as per Schuback et al. 2015), the relationship between K_C and NPQ_{NSV} further weakened for the pooled data ($R^2 = 0.22$, $p < 0.001$; Fig. 6b) likely because n_{PSII} and K_C are conflated variables. Inclusion of $[RCII]^{(FRRf)}$ thus improves predictive power of NPQ_{NSV} for this study, arguably providing further evidence that the Oxborough et al. (2012) algorithm offered improvement over the use of an assumed value for n_{PSII} within this study. We did however observe regression slopes that differed for each study month regardless of the inclusion of $[RCII]^{(FRRf)}$ (Fig 6a, b), a phenomenon also observed by Schuback et al. (2015, 2016). This discrepancy could potentially be explained by the fact that a mixed phytoplankton community was sampled at three distinct time points with varying initial environmental conditions, and thus an inherently different initial physiological state. Such subtly different physiological and taxonomic responses to nutrient addition may have culminated in variable expression of NPQ_{NSV}, or phytoplankton growth rates, which together affect the process captured by the ^{14}C-uptake method (i.e. net or gross primary production, or somewhere in between) and thus, influencing K_C. Even so, our study lends additional weight to the viability of NPQ_{NSV} as an

important parameter to improve predictive capacity of $K_{C,}$ although further study of the relationship between these two variables is clearly needed within dynamic coastal systems.

Conclusion

Nitrogen is considered the most limiting nutrient for marine primary production over much of the world's surface ocean, and hence a key factor driving variability of MPP over space and time. Through our novel bioassay-based approach to examine K_C, we have shown for the first time that N availability, in concert with other nutrients, regulates the bulk conversion of photosynthetically-generated electrons (and hence energy and reductant) to fixed carbon. Specifically, that this regulation is not only a function of N-availability itself on the physiological status of existing communities, but also in how N-availability selects for alternate phytoplankton community composition. In doing so, we have estimated the first conversion factors that can potentially be applied to future FRRf-based exercises attempting to examine C-uptake from knowledge of ETRs, the prevailing nutrient conditions and phytoplankton communities. Such a step is critical to advance the scale and application of FRRf to marine observation, particularly in physically-dynamic coastal waters. Whilst we have shown that N-availability is clearly important in regulating K_C, a critical next step will be to resolve the role of N-speciation, and interaction with bioavailability of other important macro- and micronutrients (e.g. Fe), upon this important parameter. Understanding how dynamic light fields inherent to complex coastal waters influence such interactions will be critical.

References

Ajani, P. A., A. P. Allen, T. Ingleton, and L. Armand. 2014. A decadal decline in relative abundance and a shift in microphytoplankton composition at a long-term coastal station off southeast Australia. Limnol. Oceanogr. 59(2)**:** 519-531.

Alexander, H., M. Rouco, S. T. Haley, S. T. Wilson, D. M. Karl, and S. T. Dyhrman. 2015. Functional group-specific traits drive phytoplankton dynamics in the oligotrophic ocean. Proc. Natl. Acad. Sci. 112(44)**:** E5972-E5979.

Andersen, T., T. M. Saloranta, and T. Tamminen. 2007. A statistical procedure for unsupervised classification of nutrient limitation bioassay experiments with natural phytoplankton communities. Limnol. Oceanogr.: Methods 5**:** 111-118.

Azam, F., T. Fenchel, J. Field, J. Gray, L. Meyer-Reil, and F. Thingstad. 1983. The ecological role of water-column microbes in the sea. Mar. Ecol.: Prog. Ser. 10(3)**:** 257-263.

Babin, M., A. Morel, H. Claustre, A. Bricaud, Z. Kolber, and P. G. Falkowski. 1996. Nitrogen- and irradiance-dependent variations of the maximum quantum yield of carbon fixation in eutrophic, mesotrophic and oligotrophic marine systems. Deep Sea Res., Part I. 43(8)**:** 1241-1272.

Bailey, S.and others. 2008. Alternative photosynthetic electron flow to oxygen in marine *Synechococcus*. Biochim. Biophys. Acta, Bioenerg. 1777(3)**:** 269-276.

Behrenfeld, M. J., K. Worthington, R. M. Sherrell, F. P. Chavez, P. Strutton, M. Mcphaden, and D. M. Shea. 2006. Controls on tropical Pacific Ocean productivity revealed through nutrient stress diagnostics. Nature 442(7106)**:** 1025-1028.

Berg, G. M., S. Driscoll, K. Hayashi, M. Ross, and R. Kudela. 2017. Variation in growth rate, carbon assimilation, and photosynthetic efficiency in response to nitrogen source and concentration in phytoplankton isolated from upper San Francisco Bay. J. Phycol. 53(3)**:** 664-679.

Berges, J. A., D. O. Charlebois, D. C. Mauzerall, and P. G. Falkowski. 1996. Differential effects of nitrogen limitation on photosynthetic efficiency of photosystems I and II in microalgae. Plant Physiol. 110(2)**:** 689-696.

Bergmann, T., T. Richardson, H. Paerl, J. Pinckney, and O. Schofield. 2002. Synergy of light and nutrients on the photosynthetic efficiency of phytoplankton populations from the Neuse River Estuary, North Carolina. J. Plankton Res. 24(9)**:** 923-933.

Bouchard, J., M. Longhi, S. Roy, D. Campbell, and G. Ferreyra. 2008. Interaction of nitrogen status and UVB sensitivity in a temperate phytoplankton assemblage. J. Exp. Mar. Biol. Ecol. 359(1)**:** 67-76.

Cardol, P., G. Forti, and G. Finazzi. 2011. Regulation of electron transport in microalgae. Biochim. Biophys. Acta, Bioenerg. 1807(8)**:** 912-918.

Carr, M.-E.and others. 2006. A comparison of global estimates of marine primary production from ocean color. Deep Sea Res., Part II. 53(5): 741-770.

Cheah, W., A. Mcminn, F. B. Griffiths, K. J. Westwood, S. W. Wright, E. Molina, J. P. Webb, and R. Van Den Enden. 2011. Assessing Sub-Antarctic Zone primary productivity from fast repetition rate fluorometry. Deep Sea Res., Part II. 58(21): 2179-2188.

Chisholm, S. W. 1992. Phytoplankton size, p. 213:237. In P. G. Falkowski, A. D. Woodhead and K. Vivirito [eds.], Primary productivity and biogeochemical cycles in the sea. Springer US.

Cloern, J. E., S. Foster, and A. Kleckner. 2014. Phytoplankton primary production in the world's estuarine-coastal ecosystems. Biogeosciences 11(9): 2477-2501.

Cresswell, G. 1994. Nutrient enrichment of the Sydney continental shelf. Mar. Freshwater Res. 45(4): 677-691.

Cullen, J. J., P. J. Franks, D. M. Karl, and A. Longhurst. 2002. Physical influences on marine ecosystem dynamics, p. 297-336. In A.R. Robinson, J. J. McCarthy and B. J. Rothschild [eds.], Biological-physical interactions in the sea. New York:Wiley.

Dubinsky, Z., P. G. Falkowski, and K. Wyman. 1986. Light Harvesting and utilization by phytoplankton. Plant Cell Physiol. 27(7): 1335-1349.

Dufresne, A.and others. 2003. Genome sequence of the cyanobacterium *Prochlorococcus marinus* SS120, a nearly minimal oxyphototrophic genome. Proc. Natl. Acad. Sci. 100(17): 10020-10025.

Dugdale, R., and J. Goering. 1967. Uptake of new and regenerated forms of nitrogen in primary productivity. Limnol. Oceanogr. 12(2): 196-206.

Everett, J. D., and M. A. Doblin. 2015. Characterising primary productivity measurements across a dynamic western boundary current region. Deep Sea Res., Part I. 100: 105-116.

Falkowski, P. G. 1975. Nitrate uptake in marine phytoplankton: Comparison of half-saturation constants from seven species. Limnol. Oceanogr. 20(3): 412-417.

Falkowski, P. G., R. M. Greene, and R. J. Geider. 1992. Physiological limitations on phytoplankton productivity in the ocean. Oceanography 5(2): 84-91.

Falkowski, P. G., M. E. Katz, A. H. Knoll, A. Quigg, J. A. Raven, O. Schofield, and F. Taylor. 2004. The evolution of modern eukaryotic phytoplankton. Science 305(5682): 354-360.

Falkowski, P. G., T. G. Owens, A. C. Ley, and D. C. Mauzerall. 1981. Effects of growth irradiance levels on the ratio of reaction centers in two species of marine phytoplankton. Plant Physiol. 68(4): 969-973.

Falkowski, P. G., and J. A. Raven. 2013. Aquatic photosynthesis. 2nd ed. Princeton University Press.

Field, C. B., M. J. Behrenfeld, J. T. Randerson, and P. Falkowski. 1998. Primary production of the biosphere: integrating terrestrial and oceanic components. Science 281(5374)**:** 237-240.

Fietz, S., and A. Nicklisch. 2002. Acclimation of the diatom *Stephanodiscus neoastraea* and the cyanobacterium *Planktothrix agardhii* to simulated natural light fluctuations. Photosynth. Res. 72(1)**:** 95-106.

Finkel, Z. V., and A. J. Irwin. 2000. Modeling size-dependent photosynthesis: light absorption and the allometric rule. J. Theor. Biol. 204(3)**:** 361-369.

Foster, R. A., M. M. Kuypers, T. Vagner, R. W. Paerl, N. Musat, and J. P. Zehr. 2011. Nitrogen fixation and transfer in open ocean diatom–cyanobacterial symbioses. ISME J. 5(9)**:** 1484-1493.

Gallagher, J., A. Wood, and R. Alberte. 1984. Ecotypic differentiation in the marine diatom *Skeletonema costatum*: influence of light intensity on the photosynthetic apparatus. Mar. Biol. 82(2)**:** 121-134.

Geider, R. J., R. M. Greene, Z. Kolber, H. L. Macintyre, and P. G. Falkowski. 1993. Fluorescence assessment of the maximum quantum efficiency of photosynthesis in the western North Atlantic. Deep Sea Res., Part I. 40(6)**:** 1205-1224.

Genty, B., J.-M. Briantais, and N. R. Baker. 1989. The relationship between the quantum yield of photosynthetic electron transport and quenching of chlorophyll fluorescence. Biochim. Biophys. Acta, Gen. Sub 990(1)**:** 87-92.

Giraud, M., M. Boye, V. Garçon, A. Donval, and D. De La Broise. 2016. Simulation of an artificial upwelling using immersed in situ phytoplankton microcosms. J. Exp. Mar. Biol. Ecol. 475**:** 80-88.

Halsey, K. H., A. J. Milligan, and M. J. Behrenfeld. 2010. Physiological optimization underlies growth rate-independent chlorophyll-specific gross and net primary production. Photosynth. Res. 103(2): 125-137.

Halsey, K. H., A. J. Milligan, and M. J. Behrenfeld. 2011. Linking time-dependent carbon-fixation efficiencies in *Dunaliella tertiolecta* (chlorophyceae) to underlying metabolic pathways. J. Phycol. 47(1): 66-76.

Halsey, K. H., R. T. O'malley, J. R. Graff, A. J. Milligan, and M. J. Behrenfeld. 2013. A common partitioning strategy for photosynthetic products in evolutionarily distinct phytoplankton species. New Phytol. 198(4): 1030-1038.

Hoppe, C. J. M., L.-M. Holtz, S. Trimborn, and B. Rost. 2015. Ocean acidification decreases the light-use efficiency in an Antarctic diatom under dynamic but not constant light. New Phytol. 207(1)**:** 159-171.

Huner, N. P., G. Öquist, and F. Sarhan. 1998. Energy balance and acclimation to light and cold. Trends Plant Sci. 3(6)**:** 224-230.

Irwin, A. J., Z. V. Finkel, O. M. Schofield, and P. G. Falkowski. 2006. Scaling-up from nutrient physiology to the size-structure of phytoplankton communities. J. Plankton Res. 28(5)**:** 459-471.

Killops, S., and V. Killops. 1993. Chemical composition of biogenic matter, p. 22-62. In S. D. Killops and V. J. Killops [eds.], An Introduction to Organic Geochemistry. Wiley-Blackwell.

Knap, A., A. Michaels, A. Close, H. Ducklow, and A. Dickson.1996. Protocols for the joint global ocean flux study (JGOFS) core measurements.).

Kolber, Z., and P. G. Falkowski. 1993. Use of active fluorescence to estimate phytoplankton photosynthesis in situ. Limnol. Oceanogr. 38(8)**:** 1646-1665.

Kolber, Z., J. Zehr, and P. Falkowski. 1988. Effects of growth irradiance and nitrogen limitation on photosynthetic energy conversion in photosystem II. Plant Physiol. 88(3)**:** 923-929.

Kolber, Z. S., O. Prášil, and P. G. Falkowski. 1998. Measurements of variable chlorophyll fluorescence using fast repetition rate techniques: defining methodology and experimental protocols. Biochim. Biophys. Acta, Bioenerg. 1367(1–3)**:** 88-106.

Kromkamp, J. C., and R. M. Forster. 2003. The use of variable fluorescence measurements in aquatic ecosystems: differences between multiple and single turnover measuring protocols and suggested terminology. Eur. J. Phycol. 38(2)**:** 103-112.

Lancelot, C. 1983. Factors affecting phytoplankton extracellular release in the Southern Bight of the North Sea. Mar. Ecol.: Prog. Ser. 12(2)**:** 115-121.

Laufkötter, C.and others. 2015. Drivers and uncertainties of future global marine primary production in marine ecosystem models. Biogeosciences 12**:** 6955-6984.

Lavaud, J., and P. G. Kroth. 2006. In diatoms, the transthylakoid proton gradient regulates the photoprotective non-photochemical fluorescence quenching beyond its control on the xanthophyll cycle. Plant Cell Physiol. 47(7)**:** 1010-1016.

Lavaud, J., B. Rousseau, and A. L. Etienne. 2004. General features of photoprotection by energy dissipation in planktonic diatoms (Bacillariophyceae). J. Phycol. 40(1)**:** 130-137.

Lavaud, J., C. Six, and D. A. Campbell. 2016. Photosystem II repair in marine diatoms with contrasting photophysiologies. Photosynth. Res. 127(2)**:** 189-199.

Lawrenz, E.and others. 2013. Predicting the Electron Requirement for Carbon Fixation in Seas and Oceans. PLoS One 8(3)**:** e58137.

879 Laws, E. A., and T. Bannister. 1980. Nutrient-and light-limited growth of *Thalassiosira*
880 *fluviatilis* in continuous culture, with implications for phytoplankton growth in the
881 ocean. Limnol. Oceanogr. 25(3)**:** 457-473.
882 Lippemeier, S., P. Hartig, and F. Colijn. 1999. Direct impact of silicate on the photosynthetic
883 performance of the diatom *Thalassiosira weissflogii* assessed by on-and off-line PAM
884 fluorescence measurements. J. Plankton Res. 21(2): 269-283.
885
886 Mackey, K. R. M., A. Paytan, A. R. Grossman, and S. Bailey. 2008. A photosynthetic
887 strategy for coping in a high-light, low-nutrient environment. Limnol. Oceanogr.
888 53(3)**:** 900-913.
889
890 McAndrew, P. M., K. M. Björkman, M. J. Church, P. J. Morris, N. Jachowski, P. J. L. B.
891 Williams, and D. M. Karl. 2007. Metabolic response of oligotrophic plankton
892 communities to deep water nutrient enrichment. Mar. Ecol.: Prog. Ser. 332**:** 63-75.
893
894 Milligan, A. J., K. H. Halsey, and M. J. Behrenfeld. 2015. Advancing interpretations of ^{14}C-
895 uptake measurements in the context of phytoplankton physiology and ecology. J.
896 Plankton Res. 37(4): 692-698.
897
898 Moore, C.and others. 2013. Processes and patterns of oceanic nutrient limitation. Nat. Geosci.
899 6(9)**:** 701-710.
900
901 Moore, C. M.and others. 2003. Physical controls on phytoplankton physiology and
902 production at a shelf sea front: a fast repetition-rate fluorometer based field study.
903 Mar. Ecol.: Prog. Ser. 259**:** 29-45.
904
905 Moore, C. M., M. M. Mills, R. Langlois, A. Milne, E. P. Achterberg, J. Laroche, and R. J.
906 Geider. 2008. Relative influence of nitrogen and phosphorous availability on
907 phytoplankton physiology and productivity in the oligotrophic sub-tropical North
908 Atlantic Ocean. Limnol. Oceanogr. 53(1)**:** 291-305.
909
910 Moore, C. M., D. J. Suggett, A. E. Hickman, Y.-N. Kim, J. F. Tweddle, J. Sharples, R. J.
911 Geider, and P. M. Holligan. 2006. Phytoplankton photoacclimation and
912 photoadaptation in response to environmental gradients in a shelf sea. Limnol.
913 Oceanogr. 51(2)**:** 936-949.
914
915 Morel, A., and A. Bricaud. 1981. Theoretical results concerning light absorption in a discrete
916 medium, and application to specific absorption of phytoplankton. Deep Sea Res., Part
917 I. 28(11)**:** 1375-1393.
918
919 Moreno-Madriñán, M. J., and A. M. Fischer. 2013. Performance of the MODIS FLH
920 algorithm in estuarine waters: a multi-year (2003–2010) analysis from Tampa Bay,
921 Florida (USA). Int. J. Remote Sens. 34(19)**:** 6467-6483.
922
923 Muller-Karger, F., R. Varela, R. Thunell, Y. Astor, H. Zhang, R. Luerssen, and C. Hu. 2004.
924 Processes of coastal upwelling and carbon flux in the Cariaco Basin. Deep Sea Res.,
925 Part II. 51(10)**:** 927-943.
926

Murphy, C. D., M. S. Roodvoets, E. J. Austen, A. Dolan, A. Barnett, and D. A. Campbell. 2017. Photoinactivation of Photosystem II in *Prochlorococcus* and *Synechococcus*. PloS One 12(1)**:** e0168991.

Nawrocki, W. J., N. J. Tourasse, A. Taly, F. Rappaport, and F.-A. Wollman. 2015. The plastid terminal oxidase: its elusive function points to multiple contributions to plastid physiology. Annu. Rev Plant Biol. 66**:** 49-74.

Owens, T. G., D. M. Riper, and P. G. Falkowski. 1978. Studies of delta-aminolevulinic acid dehydrase from *Skeletonema costatum*, a marine plankton diatom. Plant Physiol. 62(4)**:** 516-521.

Oxborough, K. 2012. FastPro8 GUI and FRRf3 systems documentation. West Molesey, UK: Chelsea Technologies Group Ltd.

Oxborough, K., C. M. Moore, D. J. Suggett, T. Lawson, H. G. Chan, and R. J. Geider. 2012. Direct estimation of functional PSII reaction center concentration and PSII electron flux on a volume basis: a new approach to the analysis of Fast Repetition Rate fluorometry (FRRf) data. Limnol. Oceanogr.: Methods. 10(3)**:** 142-154.

Perry, M., M. Talbot, and R. Alberte. 1981. Photoadaption in marine phytoplankton: response of the photosynthetic unit. Mar. Biol. 62(2)**:** 91-101.

Prézelin, B., G. Samuelsson, and H. Matlick. 1986. Photosystem II photoinhibition and altered kinetics of photosynthesis during nutrient-dependent high-light photoadaptation in *Gonyaulax polyedra*. Mar. Biol. 93(1)**:** 1-12.

Prihoda, J., A. Tanaka, W. B. De Paula, J. F. Allen, L. Tirichine, and C. Bowler. 2012. Chloroplast-mitochondria cross-talk in diatoms. J. Exp. Bot. 63(4)**:** 1543-1557.

Quigg, A., J. B. Sylvan, A. B. Gustafson, T. R. Fisher, R. L. Oliver, S. Tozzi, and J. W. Ammerman. 2011. Going west: nutrient limitation of primary production in the Northern Gulf of Mexico and the importance of the Atchafalaya River. Aquat. Geochem. 17(4-5)**:** 519.

Raven, J. 1997. The vacuole: a cost-benefit analysis. Adv. Bot. Res. 25**:** 59-86.

Raven, J. 1998. The twelfth Tansley Lecture. Small is beautiful: the picophytoplankton. Func. Ecol. 12(4)**:** 503-513.

Rhiel, E., K. Krupinska, and W. Wehrmeyer. 1986. Effects of nitrogen starvation on the function and organization of the photosynthetic membranes in *Cryptomonas maculata* (Cryptophyceae). Planta 169(3)**:** 361-369.

Robinson, C., D. J. Suggett, N. Cherukuru, P. J. Ralph, and M. A. Doblin. 2014. Performance of Fast Repetition Rate fluorometry based estimates of primary productivity in coastal waters. J. Mar. Syst. 139**:** 299-310.

Robinson, C.and others. 2009. Comparison of in vitro and in situ plankton production determinations. Aquat. Microb. Ecol. 54(1)**:** 13-34.

977 Roughan, M., and J. H. Middleton. 2002. A comparison of observed upwelling mechanisms
978 off the east coast of Australia. Cont. Shelf Res. 22(17)**:** 2551-2572.
979
980 Sarthou, G., K. R. Timmermans, S. Blain, and P. Tréguer. 2005. Growth physiology and fate
981 of diatoms in the ocean: a review. J. Sea Res. 53(1)**:** 25-42.
982
983 Schuback, N., M. Flecken, M. T. Maldonado, and P. D. Tortell. 2016. Diurnal variation in the
984 coupling of photosynthetic electron transport and carbon fixation in iron-limited
985 phytoplankton in the NE subarctic Pacific. Biogeosciences 13(4)**:** 1019-1035.
986
987 Schuback, N., C. J. Hoppe, J. É. Tremblay, M. T. Maldonado, and P. D. Tortell. 2017.
988 Primary productivity and the coupling of photosynthetic electron transport and carbon
989 fixation in the Arctic Ocean. Limnol. Oceanogr. 62(3): 898-921.
990
991 Schuback, N., C. Schallenberg, C. Duckham, M. T. Maldonado, and P. D. Tortell. 2015.
992 Interacting effects of light and iron availability on the coupling of photosynthetic
993 electron transport and CO_2-assimilation in marine phytoplankton. PLoS One 10(7)**:**
994 e0133235.
995
996 Sciandra, A.and others. 1997. Growth-compensating phenomena in continuous cultures of
997 *Dunaliella tertiolecta* limited simultaneously by light and nitrate. Limnol. Oceanogr.
998 42(6)**:** 1325-1339.
999
1000 Shrestha, R. P., B. Tesson, T. Norden-Krichmar, S. Federowicz, M. Hildebrand, and A. E.
1001 Allen. 2012. Whole transcriptome analysis of the silicon response of the diatom
1002 *Thalassiosira pseudonana*. BMC Genomics 13(1)**:** 499.
1003
1004 Silsbe, G. M.and others. 2015. Toward autonomous measurements of photosynthetic electron
1005 transport rates: An evaluation of active fluorescence-based measurements of
1006 photochemistry. Limnol. Oceanogr.: Methods. 13(3)**:** 138-155.
1007
1008 Smyth, T. J., K. L. Pemberton, J. Aiken, and R. J. Geider. 2004. A methodology to determine
1009 primary production and phytoplankton photosynthetic parameters from Fast
1010 Repetition Rate Fluorometry. J. Plankton Res. 26(11)**:** 1337-1350.
1011
1012 Suggett, D., G. Kraay, P. Holligan, M. Davey, J. Aiken, and R. Geider. 2001. Assessment of
1013 photosynthesis in a spring cyanobacterial bloom by use of a fast repetition rate
1014 fluorometer. Limnol. Oceanogr. 46(4)**:** 802-810.
1015
1016 Suggett, D. J., H. L. Macintyre, and R. J. Geider. 2004. Evaluation of biophysical and optical
1017 determinations of light absorption by photosystem II in phytoplankton. Limnol.
1018 Oceanogr.: Methods. 2(10)**:** 316-332.
1019
1020 Suggett, D. J., H. L. Macintyre, T. M. Kana, and R. J. Geider. 2009. Comparing electron
1021 transport with gas exchange: parameterising exchange rates between alternative
1022 photosynthetic currencies for eukaryotic phytoplankton. Aquat. Microb. Ecol. 56(2-
1023 3)**:** 147-162.
1024

Suggett, D. J., C. M. Moore, A. E. Hickman, and R. J. Geider. 2009. Interpretation of fast repetition rate (FRR) fluorescence: signatures of phytoplankton community structure versus physiological state. Mar. Ecol.: Prog. Ser. 376**:** 1-19.

Tamminen, T., and T. Andersen. 2007. Seasonal phytoplankton nutrient limitation patterns as revealed by bioassays over Baltic Sea gradients of salinity and eutrophication. Mar. Ecol.: Prog. Ser. 340**:** 121-138.

Thompson, P., M. Baird, T. Ingleton, and M. Doblin. 2009. Long-term changes in temperate Australian coastal waters: implications for phytoplankton. Mar. Ecol.: Prog. Ser. 394**:** 1-19.

Tilman, D., S. S. Kilham, and P. Kilham. 1982. Phytoplankton community ecology: the role of limiting nutrients. Annu. Rev. Ecol. Syst. 13(1)**:** 349-372.

Villareal, T. A., C. G. Brown, M. A. Brzezinski, J. W. Krause, and C. Wilson. 2012. Summer diatom blooms in the North Pacific subtropical gyre: 2008–2009. PLoS One 7(4)**:** e33109.

Welschmeyer, N. A., and C. J. Lorenzen. 1984. Carbon-14 labeling of phytoplankton carbon and chlorophyll a carbon: Determination of specific growth rates. Limnol. Oceanogr 29(1)**:** 135-145.

Werner, D. 1977. Silicate metabolism. In D. Werner [ed.], The biology of diatoms. University of California Press.

White, S., A. Anandraj, and F. Bux. 2011. PAM fluorometry as a tool to assess microalgal nutrient stress and monitor cellular neutral lipids. Bioresour. Technol. 102(2)**:** 1675-1682.

Wilhelm, C.and others. 2006. The regulation of carbon and nutrient assimilation in diatoms is significantly different from green algae. Protist 157(2)**:** 91-124.

Wilkerson, F. P., R. C. Dugdale, V. E. Hogue, and A. Marchi. 2006. Phytoplankton blooms and nitrogen productivity in San Francisco Bay. Estuaries Coasts 29(3)**:** 401-416.

Wilson, K. E., and N. P. Huner. 2000. The role of growth rate, redox-state of the plastoquinone pool and the trans-thylakoid ΔpH in photoacclimation of *Chlorella vulgaris* to growth irradiance and temperature. Planta 212(1)**:** 93-102.

Wu, Y., J. Jeans, D. J. Suggett, Z. V. Finkel, and D. A. Campbell. 2014. Large centric diatoms allocate more cellular nitrogen to photosynthesis to counter slower RUBISCO turnover rates. Front. Mar. Sci. 1**:** 68.

Young, E. B., and J. Beardall. 2003. Photosynthetic function in *Dunaliella tertiolecta* (Chlorophyta) during a nitrogen starvation and recovery cycle. J. Phycol. 39(5)**:** 897-905.

Zhao, Y., Y. Wang, and A. Quigg. 2015. The 24 hour recovery kinetics from N starvation in *Phaeodactylum tricornutum* and *Emiliania huxleyi*. J. Phycol. 51(4)**:** 726-738.

Zhu, Y., J. Ishizaka, S. C. Tripathy, S. Wang, Y. Mino, T. Matsuno, and D. J. Suggett. 2016. Variation of the photosynthetic electron transfer rate and electron requirement for daily net carbon fixation in Ariake Bay, Japan. J. Oceanogr. 72(5)**:** 761-776.

Acknowledgements

The authors would like to thank the crew of the RV Zelda Faith for their support during the sampling campaign. We also wish to acknowledge invaluable insight from Penny Ajani regarding phytoplankton identification and enumeration. Rhianne Oliver, Paul Brooks, Sue Fenech, Marco Alvarez and Arjun Verma provided technical support and advice at various stages during the experiment. We also acknowledge valuable discussions across the peer community in distilling the concepts presented here; in particular, we thank Kevin Oxborough, Doug Campbell and Mark Moore. Also, we are extremely grateful to insightful comments provided by two anonymous reviewers to help further improve the manuscript. The contribution of DJS was via an ARC Future Fellowship (FT130100202), and input of MD and DJS enhanced through involvement with an ARC Linkage Infrastructure, Equipment and Facilities project LE160100146 led by David Antoine. Data presented in Figure 2 was supported by the CSIRO Marine and Coastal Carbon Biogeochemistry Cluster and Australia's Integrated Marine Observing System (IMOS).

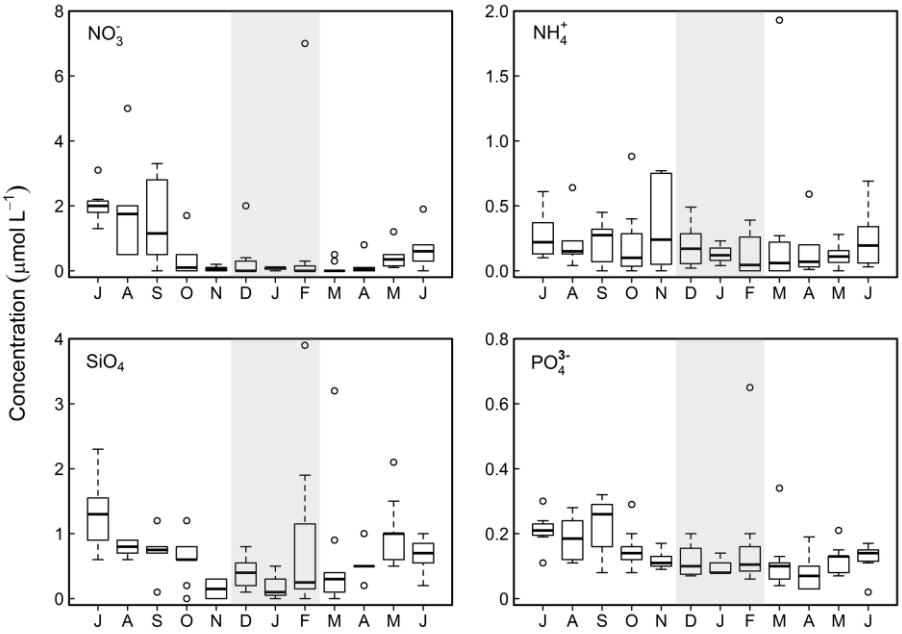

Figure 1 Box plots of monthly dissolved nutrient concentrations, nitrate, ammonia, silicate and phosphorus in units of µmol L^{-1}, recorded at the Port Hacking 100m National Reference Station (PH_{100m}), NSW, Australia. Data encompasses measurements performed from 2005-2013. For each sample, the median is indicated by the bold line and the large box indicates the inter-quartile range (1st to 3rd quartiles). Box and whiskers represent 95% of data range associated with each sample, whilst open circles denote outliers. Months are shown from July-June on the x-axis for easier interpretation of austral summer sampling period (highlighted by shaded area). **Note the different scales on the y-axis, reflecting variability in magnitude of respective nutrient pools.** Nutrient data presented was made publicly available by the IMOS ocean data portal (http://imos.aodn.org.au).

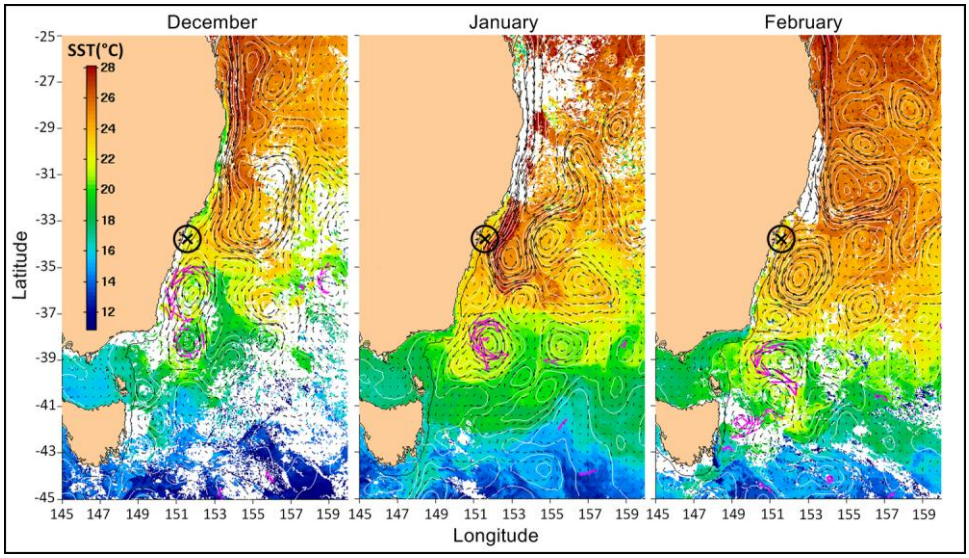

1116

1117

1118 **Figure 2** Satellite images of NSW-IMOS region for the three sampling dates in this study (9th

1119 December 2014, 22nd January 2015 and 26th February 2015) showing remotely-sensed sea

1120 surface temperature (SST), from which the influence of the Eastern Australian Current (EAC)

1121 upon our sampling site can be inferred. Location of the Port Hacking 100m mooring

1122 (PH_{100m}) is indicated by site marker (black X). Pink arrows denote drifter velocity data,

1123 obtained from the Surface Velocity Program (SVP), a Lagrangian current-following drifter

1124 situated at approximately 15m depth. Geostrophic velocity is denoted by small black arrows.

1125 Data presented is publically-available and was accessed via the IMOS ocean data portal

1126 (http://imos.aodn.org.au).

1127

1128

1129

1130

1131

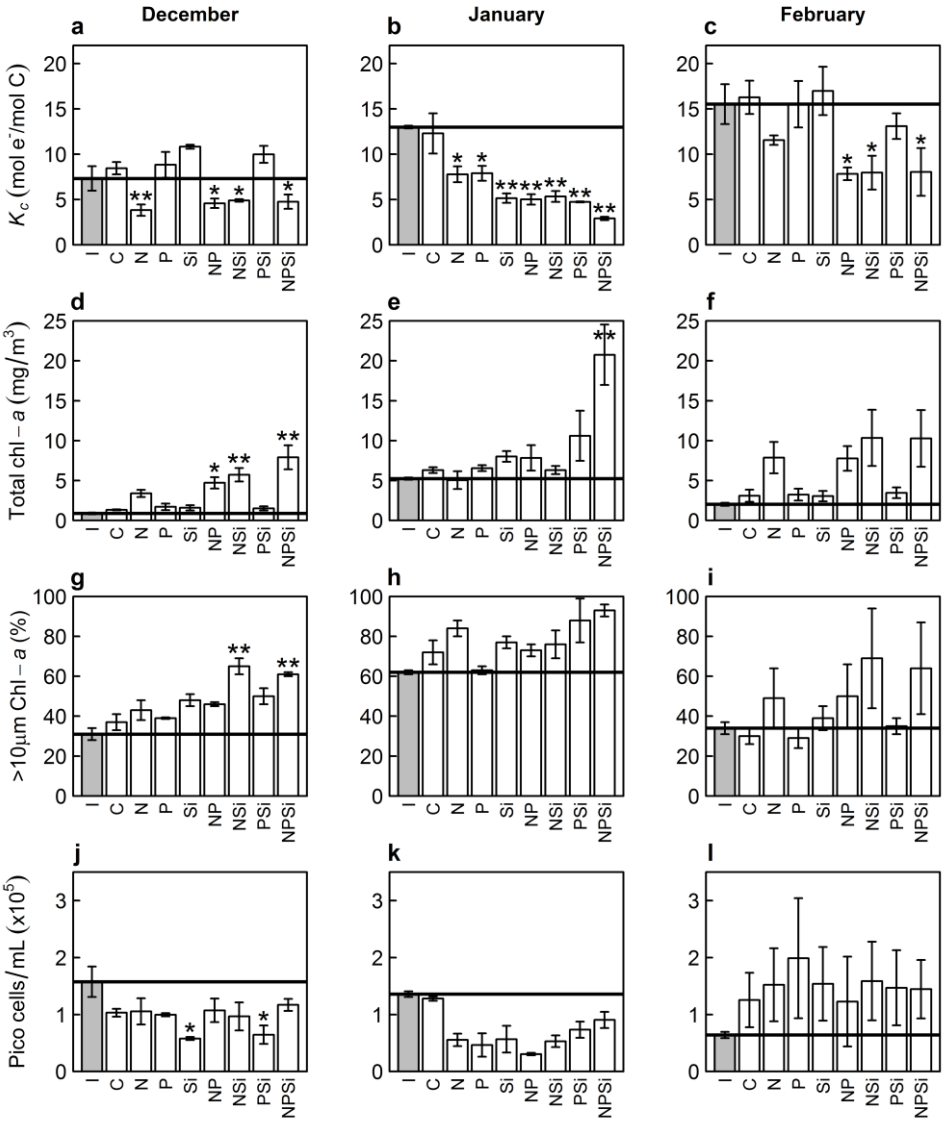

Figure 3 Initial (I) and final concentrations after 60 hours of K_C **(a-c)**, total Chlorophyll-*a* (Chl-*a*) concentration **(d-f)**, >10 µm size-fractionated Chl-*a* **(g-i)** and picophyoplankton abundance **(j-l)** to the addition of different nutrient combinations for three austral-summer months. Error bars indicate standard errors (n=3) and solid black line denotes the initial value (error is indicated on grey bar). * and ** denote statistical differences ($p < 0.05$ and 0.01 respectively) between the treatment and control (C) (one-way ANOVA, Dunnett's post-hoc test).

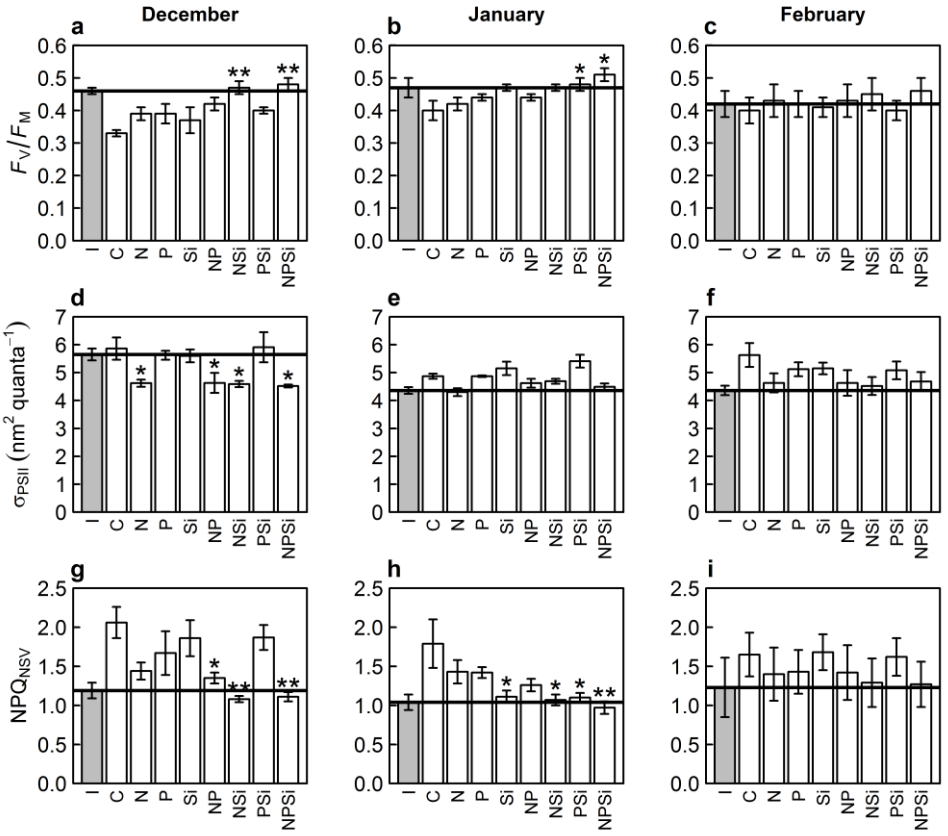

1141

1142

1143 **Figure 4** Photophysiological responses of F_v/F_m **(a-c)**, functional absorption cross section of
1144 PSII (σ_{PSII}) **(d-f)**, and non-photochemical quenching, calculated as normalised Stern-Volmer
1145 quenching, (NPQ_{NSV}) **(g-i)** to the addition of different nutrient combinations for three austral-
1146 summer months. Solid black line denotes the initial value (error is indicated on grey bar). *
1147 and ** denote statistical differences ($p < 0.05$ and 0.01 respectively) between the treatment
1148 and control (C) (ANOVA).

1149

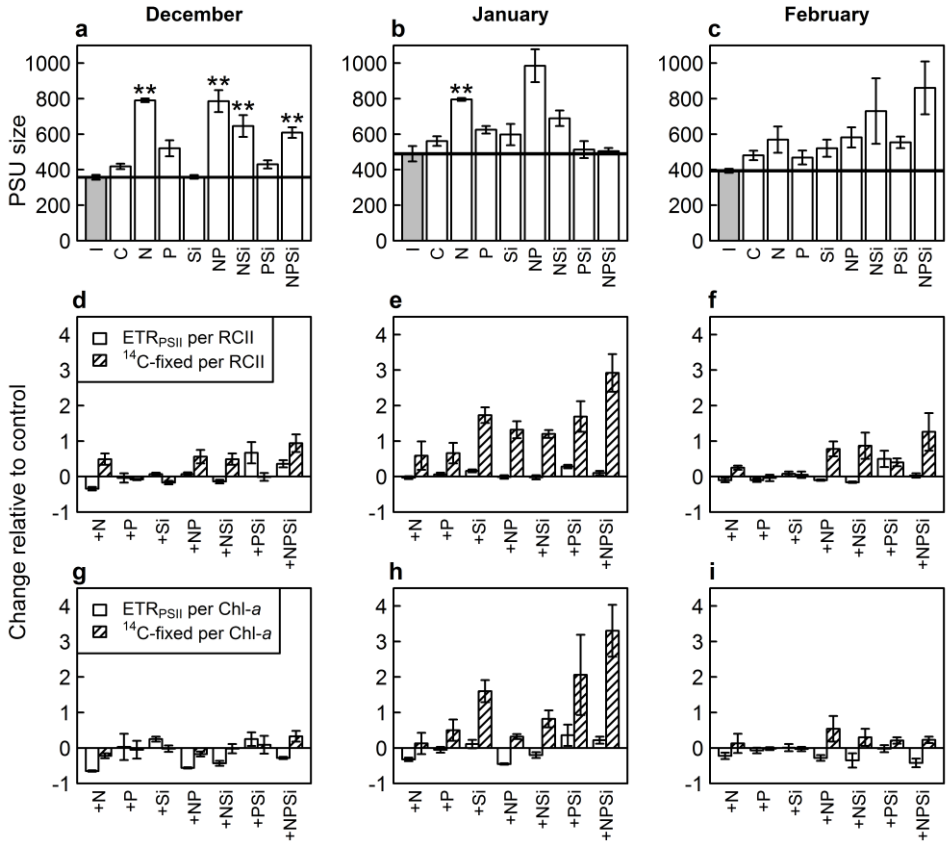

Figure 5 Response of photosynthetic unit (PSU) size (mol Chl-*a* [mol RCII]) to the addition of different nutrient combinations for three austral-summer months (**a-c**). Also shown is the relative change in ETR_{PSII} and C-uptake normalised to both PSII reaction centre (RCII) concentration (**d-f**) and Chlorophyll-*a* concentration (**g-i**) for all treatments relative to the control. ** denote statistical differences ($p < 0.01$) between the treatment and control (C) (ANOVA).

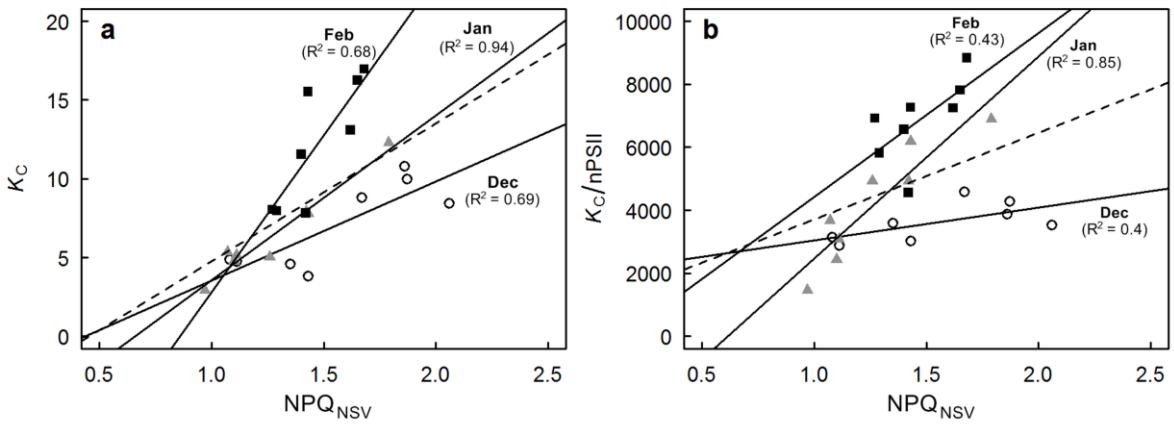

1159

1160 **Figure 6** Relationship between **a)** the electron requirement for carbon fixation (K_C) and the
1161 expression of non-photochemical quenching (NPQ_{NSV} calculated as per Oxborough, 2012)
1162 and **b)** K_C/n_{PSII} against NPQ_{NSV} (i.e. without estimation of Photosynthetic Unit [PSU] size
1163 following the approach of Schuback et al. 2015). Data shown is for December (open circles)
1164 January (grey triangles) and February (closed squares). The dotted regression line represents
1165 the pooled data (R^2=0.41 and R^2=0.22 for **a** and **b** respectively). NPQ_{NSV} reflects an
1166 integrated value from 5 minute FRRf incubations under 104 µmol photons m^{-2} s^{-1}.

1167

1168

1169

1170

1171

1172

1173

Table 1 Abbreviations and definitions used throughout the main text. For active fluorescence parameters the prime notation (′) denotes that measurements are performed under actinic light, whilst unprimed denotes that measurements were performed in a dark-adapted state.

Abbreviation	Definition
FRRf	Fast Repetition Rate fluorometry
K_C	Electron requirement for carbon fixation (mol e^- [mol C]$^{-1}$)
PSII	Photosystem II
[RCII]	Concentration of PSII reaction centres
$[RCII]^{(FRRF)}$	Concentration of [RCII] as estimated by FRRf
LEF	Linear electron flow
AEF	Alternative electron flow
ETR_{PSII}	Electron transfer rate through photosystem II
Chl-*a*	Chlorophyll *a*
n_{PSII}	Ratio of PSII reaction centres per unit Chl-*a*
F'	Fluorescence yield under actinic light at time *t*
$F_0(')$	Minimum PSII Fluorescence yield
$F_m(')$	Maximum PSII Fluorescence yield
F_v/F_m	Maximum photochemical efficiency (dark-adapted)
F_v'/F_m'	Maximum photochemical efficiency (light-adapted)
σ_{PSII}	Functional absorption cross-section of PSII
$\sigma_{PSII}(')$	Functional absorption cross-section of PSII (under actinic light)
q*P*	Photochemical quenching parameter
$\rho(')$	PSII connectivity factor (under actinic light)
NPQ	Non-photochemical quenching
NPQ_{NSV}	NPQ (estimated as normalized Stern-Volmer quenching)
MPP	Marine primary production

Table 2 Initial conditions for bioassay experiments. Mean (±SE) of triplicate samples where applicable. *Further taxonomic breakdown of dominant phytoplankton group is presented in Table 3. **denotes average taken from historic February measurements due to loss of sample from this particular month. Sea Surface temperature corresponds to value recorded by the conductivity, temperature and depth (CTD) sensor deployed from the Research Vessel (RV) Zelda Faith during sampling.

	December	**January**	**February**
Sampling Date	09/12/2014	22/01/2015	26/02/2015
Sea Surface Temperature (°C)	21.6	23.3	23.5
Mixed Layer Depth (m)	16	10.5	25
Local Weather Conditions	Overcast	Clear	Overcast
Sunrise/Sunset (AET)	05:37 / 19:58	06:06 / 20:08	06:40 / 19.37
Salinity (ppt)	35.60	35.26	35.35
Dissolved inorganic carbon (µmol kg^{-1})	2330.39	2318.12	2325.00**
NO^3 (µmol L^{-1})	< detection limit	0.1	< detection limit
NH_4 (µmol L^{-1})	0.39	0.23	0.05
PO_4 (µmol L^{-1})	0.07	0.14	0.12
Si (µmol L^{-1})	0.7	0.5	Below detection limit
Dominant >10 µm phytoplankton group*	Diatoms	Diatoms, Dinoflagellates	Diatoms
Picocyanobacteria (x 10^4 cells mL^{-1})	15.2 ± 2.5	8.5 ± 0.1	5.3 ± 0.5
Picoeukaryotes (x 10^3 cells mL^{-1})	5.5 ± 0.1	50.3 ± 0.5	11.6 (1.2)

Table 3 Predominant taxa (nano- and microphytoplankton) identified by microscopy for initial samples, and after 60 hour incubation for control and nutrient treatments. The top three genera for each treatment are shown, and their relative abundance (%), along with their functional group: (**Cya**nobacterium, **Dia**tom, **Din**oflagellate, **Fla**gellate and **Hap**tophyte). Values represent the mean of triplicates (3 x 250 mL samples) where a minimum of 100 cells were counted for each bottle with the exception of the December controls (91 total cells counted across the pooled triplicate bottles). *[1,2,3] denotes that a particular genus was only found in the carboy indicated by superscript number.

	December	January	February
Initial	*Nitzschia* (22%) **Dia** *Leptocylindrus* (17%) **Dia** *Chaetoceros* (11%) **Dia**	*Leptocylindrus* (23%) **Dia** *Prorocentrum* (15%) **Din** *Chaetoceros* (15%) **Dia** *Protoperidinium* (12%) **Din**	*Leptocylindrus* (68%) **Dia** *Rhizoselenia* (5%) **Dia** Unidentified (4%) **Din**
Control	*Nitzschia* (31%) **Dia** *Leptocylindrus* (16%) **Dia** *Ceratium* (8%) **Din**	*Leptocylindrus* (25%) **Dia** *Protoperidinium* (19%) **Din** *Prorocentrum* (14%) **Din**	*Leptocylindrus* (71%) **Dia** Unidentified (8%) **Din** *Rhizoselenia* (5%) **Dia**
+N	*Skeletonema* (34%) **Dia** *Nitzschia* (17%) **Dia** *Leptocylindrus* (15%) **Dia**	*Leptocylindrus* (45%) **Dia** *Chaetoceros* (38%) **Dia** *Nitzschia* (7%) **Dia**	*Leptocylindrus* (51%) **Dia** Unidentified (20%) **Fla*[3]** *Skeletonema* (5%) **Dia**
+P	*Leptocylindrus* (38%) **Dia** *Nitzschia* (26%) **Dia** *Skeletonema* (6%) **Dia**	*Leptocylindrus* (45%) **Dia** *Chaetoceros* (23%) **Dia** *Nitzschia* (16%) **Dia**	*Leptocylindrus* (67%) **Dia** Unidentified (16%) **Hap** Unidentified (7%) **Fla**
+Si	*Leptocylindrus* (34%) **Dia** *Trichodesmium* (23%)*[1] **Cya** *Skeletonema* (22%) **Dia**	*Leptocylindrus* (48%) **Dia** *Nitzschia* (16%) **Dia** *Chaetoceros* (16%) **Dia**	*Leptocylindrus* (83%) **Dia** *Rhizoselenia* (3%) **Dia** *Proboscia* (2%) **Dia**
+NP	*Nitzschia* (64%) **Dia** *Leptocylindrus* (16%) **Dia** *Skeletonema* (10%) **Dia**	*Skeletonema* (37%) **Dia** *Leptocylindrus* (26%) **Dia** *Nitzschia* (15%) **Dia**	*Leptocylindrus* (62%) **Dia** *Skeletonema* (22%) **Dia** *Rhizoselenia* (5%) **Dia**
+NSi	*Leptocylindrus* (56%) **Dia** *Nitzschia* (16%) **Dia** *Chaetoceros* (5%) **Dia**	*Skeletonema* (36%) **Dia** *Chaetoceros* (24%) **Dia** *Leptocylindrus* (23%) **Dia**	*Leptocylindrus* (71%) **Dia** Unidentified (8%) **Fla** Unidentified (6%) **Hap**
+PSi	*Leptocylindrus* (50%) **Dia** *Nitzschia* (36%) **Dia** *Skeletonema* (3%) **Dia**	*Leptocylindrus* (40%) **Dia** *Skeletonema* (23%) **Dia** *Chaetoceros* (11%) **Dia**	*Leptocylindrus* (87%) **Dia** *Skeletonema* (3%) **Dia** Unidentified (3%) **Fla**
+NPSi	*Nitzschia* (52%) **Dia** *Leptocylindrus* (31%) **Dia** *Chaetoceros* (3%) **Dia**	*Skeletonema* (55%) **Dia** *Leptocylindrus* (17%) **Dia** *Chaetoceros* (10%) **Dia**	*Leptocylindrus* (49%) **Dia** *Skeletonema* (38%) **Dia** *Chaetoceros* (3%) **Dia**